공학박사 학위논문

Functional Surface Coating on Magnesium to Improve Corrosion Resistance and Biocompatibility for Biodegradable Medical Applications

기능성 표면 코팅을 통한 의료용 생분해성 마그네슘 임플란트의 부식저항성 및 생체친화성 증진

2017년 8월

서울대학교 대학원

재료공학부

강 민 호

Abstract

Functional Surface Coating on Magnesium to Improve Corrosion Resistance and Biocompatibility for Biodegradable Medical Applications

Min-Ho Kang

Department of Materials Science and Engineering

Seoul National University

Biodegradable implants were suggested as an ideal biomedical implant due to the elimination of a second surgery to remove the devices after the healing of the surrounding tissues. Magnesium (Mg) and its alloys have gained considerable attention as a promising biomaterial for biodegradable implants due to the outstanding mechanical properties and biocompatibility, especially in dental, orthopedic and vascular stent applications. However, despite the significant advantages of Mg, the excessively high corrosion rate of Mg and its alloys is one of the major drawbacks for clinical use of Mg-

based implants. Therefore, in order to not only decrease the degradation rate but also enhance the biological responses to improve the function of the implant, various functional surface treatments have been performed.

In the first study, PEI-Silica hybrid coated biomimetic Mg was fabricated for dental and orthopedic application. By mimicking the structure and component of the bone, biodegradable Mg implant with high strength and pore interconnectivity and good osteoconductivity can be acquired. Bone has structure with combined dense and porous structure resulting in high strength/density ratio. Furthermore, it is composed with hydroxyapatite (HA) which has excellent osteoconductivity. By spark plasma sintering and space holder process Mg scaffold with combined dense/porous structure can be fabricated. Due to the bone-mimicking structure, Mg implant can have high strength and stiffness with high pore interconnectivity. Moreover, by controlling the ratio of dense structure, mechanical strength and stiffness can be controlled. By aqueous precipitation coating method HA can be coated on the Mg implant. This HA layer can enhance both corrosion resistance and biocompatibility with osteoblast cells. However, cracks form on HA coating layer due to the brittle property of HA. These cracks could be critical in corrosion and biological behavior on porous Mg due to complex shape and large surface area. Consequently, PEI-Silica hybrid layers were dual coated on

the bone-mimetic Mg. Due to the high corrosion resistance of PEI and excellent bioactivity of silica, corrosion rate of bone-mimetic Mg decreased remarkably and both biocompatibility and bioactivity with bone tissue were enhanced. Thus, PEI-Silica hybrid coated biomimetic Mg implant could be a promising biodegradable scaffold for dental and orthopedic applications.

In the second study, selective PEI/PLGA dual layer was coated on Mg for the biodegradable drug eluting stent application. Corrosion rate of Mg stent is need to be slowed down to maintain the scaffolding ability until the revascularization has been finished. Moreover, anti-proliferative drug is needed to be released to prohibit restenosis. To achieve these needs, Mg stent was selectively coated with PEI/PLGA dual layer by spray coating process. PEI was fully coated on the surface of the Mg stent to decrease the fast corrosion rate and improve the biocompatibility with endothelial cells. Subsequently, sirolimus loaded PLGA was selectively coated on abluminal side of the Mg stent to control the release of the drug to the wall of the blood vessel. This selective drug release can prohibit the proliferation of smooth muscle cells and prohibit the anti-proliferative effect to endothelial cell on luminal side of the Mg stent. Thus, selective PEI/PLGA dual coating on Mg stent offers a promising approach for the development of biodegradable drug eluting vascular stent application.

In conclusion, these researches were about improving the functions of the Mg implant by enhancing the corrosion resistance and biocompatibility with stable surface coatings for various biomedical applications. The degradation tests and *in-vitro* cell tests showed the PEI-Silica hybrid coating and selective PEI/PLGA dual coating had effectively enhanced corrosion protection and cellular responses of Mg implant offering excellent function for dental/orthopedic application and vascular stent application respectively.

Keywords: Magnesium (Mg); Surface coating; Corrosion resistance; Biocompatibility; Bioactivity; Hydroxyapatite (HA); Poly(ether imide) (PEI); Silica nanoparticle; Porous scaffold; Poly(lactic-co-glycolic acid) (PLGA); Stent;

Student number: 2011-23308

Contents

List of Tables

List of Figures

Chapter 1.

Introduction (Theoretical Review)

1.1. Potential of Mg for biodegradable implants

Biodegradable implants were suggested as an ideal biomedical implant due to the elimination of a second surgery to remove the devices after healing of the surrounding tissues [2]. For example, poly(glycolide) (PGA), poly(caprolactone) (PCL), poly(L-lactide) (PLA) and their copolymers were suggested as a polymer for biodegradable implant due to the non-toxic and biocompatible property [2]. However, due to the poor mechanical properties compared with those of the biodegradable metallic materials, these polymeric materials were limited to be applied actively for the medical applications [3-5]. Moreover, a local inflammation was found occasionally during the degradation process of the biodegradable polymer implants [2].

A magnesium (Mg) and its alloys were actively applied in an engineering field due to high strength to weight ratio, high thermal conductivity, and good machinability [6, 7]. Recently, magnesium and its alloys have gained considerable attention as a promising biodegradable implant due to its outstanding mechanical properties and biological performances. Moreover, in contrast with other metallic materials, Mg has comparable density (1.74-2.0 g/cm^3) and elastic modulus (41-45 GPa) to those of human natural bone (1.8-2.1 g/cm^3, 3-20 GPa) as shown in Table 1.1., thus minimizing stress-shielding effects [1, 5, 8]. In biological performance, it was

explained that during the degradation of Mg implant non-toxic by-products are formed and can be tolerated by the human body without any harmful effect [5, 9]. It is because degradation products are likely to be excreted readily through the kidney [1, 5, 8, 10]. Moreover, degradation products are also known to stimulate bone growth, accelerating bone regeneration by stimulating a hydroxyapatite (HA) formation which is one of the main component of the bone [8].

1.2. Limitation of Mg in physiological environment

Despite the excellent properties of Mg, the rapid corrosion rate of Mg and its alloys is one of the major drawbacks for clinical use of Mg-based implants [1, 5, 11, 12]. Mg forms a slightly soluble magnesium hydroxide ($Mg(OH)_2$) in a water which is passivation layer of the Mg, inducing it to be degraded slowly. As shown in the redox potential pH-value diagram (Figure 1.1.), the $Mg(OH)_2$ can be degraded when the pH value is lower than 10 [13]. Therefore, in physiological conditions, the pH of the human body cannot exceed 10, making the Mg possible as the biodegradable material.

Nonetheless, the Mg degradation rate would be faster in a

physiological condition which has high chloride (Cl^-) concentration [12, 14]. The reason is that the passivation layer of $Mg(OH)_2$ easily reacts with Cl^-, forming a highly soluble magnesium chloride ($MgCl_2$) and hydrogen gas (H_2). Considering the fact that a pitting corrosion occurs in the 30 mmol/L of Cl^- concentration, the degradation would be accelerated in the physiological environment with higher concentration of Cl^- (150 mmol/L Cl^-). These reactions are summarized and illustrated by a following chemical reaction formula and schematic diagram as shown in Figure 1.2. [4, 15].

$$Mg_{(s)} + 2H^+_{(aq)} + 2H_2O \rightarrow Mg^{2+}_{(aq)} + 2OH^-_{(aq)} + H_{2(g)}$$

$$Mg^{2+}_{(aq)} + 2OH^-_{(aq)} \rightarrow Mg(OH)_{2(s)}$$

$$Mg(OH)_{2(s)} + 2Cl^-_{(aq)} \rightarrow MgCl_{2(aq)} + 2OH^-_{(aq)}$$

The fast degradation of the Mg prohibits the bone regeneration and defect healing. Moreover, it was reported that the by-products formed during the rapid degradation caused serious problems. The accumulated hydrogen gas could delay healing and occur necrosis of near tissue by separating tissue and tissue's layers [4]. Furthermore, the radical increase of pH also resulted in the chronic local inflammatory, alkaline poisoning effect [4].

1.3. Surface coating to control the corrosion of Mg

1.3.1. Surface coating

Surface coating is one of the excellent process as it shows better performance in decreasing the degradation rate of Mg and improving its bioactivity while maintaining the inherent mechanical properties of Mg implant. Ideal surface coating on Mg implant would slow down the corrosion to maintain the mechanical integrity of the metal implant during tissue healing as shown in Figure 1.3. By slowing down the corrosion of Mg implant, hydrogen evolution and increase of pH, which have been observed as potential dangerous corrosion by-product, would be restrained. The slow wear away or degradation of coatings allow the control of degradation rate of Mg implant [16]. A various coating techniques and coating materials depending on the applications are another attractiveness of surface coating. Various coating techniques such as the chemical conversion, alkali heat treatment, anodic and micro arc oxidation, electrodeposition, and sol-gel methods were researched and applied in various applications. Furthermore, for the coating materials of biomedical application many studies focus on bio-ceramics, in particular calcium phosphate group, and bio-polymers, due to their good

corrosion resistance and biocompatibility [16-18].

1.3.2. Bio-ceramic coating

Bio-ceramics, in particular calcium phosphate, have many attractive properties for coating material in biomedical application since they have excellent corrosion resistance and biocompatibility [19-22]. They have a similar chemical composition and architecture to those of the mineral component of bones, resulting in less immune response and excellent biocompatibility with osseous tissues. Due to these properties calcium phosphate based bio-ceramics are often used in bone related biomedical application, integrating into living tissues and actively remodeling healthy bones [23]. In consequence, bio-ceramic coating particularly calcium phosphate coatings are of special interest for surface modification of Mg in dental and orthopedic applications in terms of excellent corrosion protection and bioactivity.

Various calcium phosphate based bio-ceramic coatings have been applied in various techniques showing great potential for biomedical applications. Among various methods simple chemical immersion techniques have been researched to coating calcium phosphate on Mg implant. Zhang et al. have introduced the hydroxyapatite (HA) coatings which is a component of the bone by immersing pure Mg into three times concentrated simulated body

fluid (SBF) for 24 h at 42 °C [22]. By the HA coating corrosion rate of Mg has been decreased and as the thickness of HA coatings layer increased by longer immersion time in SBF the corrosion slowed down further. Yang et al. have also introduced HA coating technique by immersing Mg in supersaturated calcification solution containing $Ca(NO)_3$, NaH_2PO_4, and $NaHCO_3$ at 37 °C for 48 h, followed by 2 h heat treatment at 300 °C [16]. Corrosion of Mg has been remarkably restrained and Ca/P contents in HA coating decreased showing the degradation of the HA coating layer.

Micro-arc oxidation (MAO) is one of the effective method to coat with uniform coating layer and high surface area. MAO is performed in electrolyte with calcium and phosphorus ions with a high voltage spark treatment occurring electrochemical oxidation to coat Mg. Srinivasan et al. have performed MAO using the $Ca(OH)_2$ and Na_3PO_4 electrolytes with different mass ratios to coat on AM50 alloys [24]. Coating layers on AM50 were constituted with MgO and $Mg_3(PO_4)_2$ and the phase composition was influenced by the phosphate ion concentration and conductivity of the electrolyte.

Furthermore, calcium phosphate with different compositions have been researched for the better performances in biological response. Ravazi et al have introduced fluoridated HA (FHA) coating on micro-arc oxidized AZ91

alloy by electrophoretic deposition (EPD) [25]. By performing *in-vivo* tests, a significant enhancement in the corrosion resistance and biocompatibility of FHA/MAO coated Mg compared to the uncoated one were shown. Moreover, new bone was formed around the coated implant with less inflammation, showing the FHA/MAO coated implant would be a suitable candidate for future clinical biomedical applications. Furthermore, Wang et al. suggested a Ca deficient HA coating on Mg by pulse electrodeposition process using positive and reverse currents [26]. The coating layer slowed down the corrosion of Mg and improved bone regeneration [27]. Moreover, this technique was reported to significantly improve the bonding strength between coating and substrate to (41.8 ± 2.7) MPa [26].

1.3.3. Bio-polymer coating

Bio-polymers are another promising candidate for the coating material on Mg implant due to the various chemical and physical functions they can offer. Bio-polymers already have been used in various biomedical applications such as membranes, drug carrier, contact lenses, catheters, breast implants, bone screws, etc [28]. In consequences, researchers have focused on polymer coatings due to the performances of bio-polymers, such as biocompatibility, elasticity and biodegradability, etc. Moreover, the degradable polymer

coatings, such as poly(caprolactone) (PCL), poly(L-lactic acid) (PLLA), and poly(DL-lactic-co-glycolide) (PLGA), have been getting attention due to the ideal function in biodegradable Mg coating material which protect the Mg implant in the early stage and gradually degrade [17]. Thus various polymer based coatings have been applied in different methods to improve the corrosion resistance of Mg substrate.

Spin coating technique is one of the simplest and fastest method to coat polymer in uniform thickness. Xu et al. have prepared the uniform and non-porous PCL and PLLA coatings on Mg substrate using spin coating technique [29, 30]. The PLLA coating provided better protection and bonding to Mg substrate than the PCL coating. Furthermore, polymer coating with lower molecular weight had lower bonding strength with Mg substrate results in faster corrosion than polymer coatings with the high molecular weight.

Alternatively, dip coating is one of the effective method to apply polymer coatings on complex shaped implants. Diez et al. have prepared a PLLA dual coating on HA coated WE43 alloy by dip coating method with a coating thickness of 3 μm for both HA and PLLA [31]. The additional PLLA coating layer provided good protection to the HA coated WE43 alloy from corrosion regardless of deformation. Gu et al. have applied the chitosan dip coating on Mg-Ca alloy and found that the performances of chitosan coating

depends on the molecular weight of the chitosan and the number of coating cycles [32].

Additionally, Wong et al. sprayed the PCL solution on the AZ91 alloy layer by layer and the porous polymer membrane was obtained [33]. The porosity of the PCL membrane was related to the PCL concentrations and thus influenced the corrosion behavior. The *in-vitro* and *in-vivo* corrosion tests indicated that the AZ91D with low porosity coatings exhibited slower corrosion rate than that with high porosity coatings.

Likewise, several materials and techniques were applied to Mg and Mg alloys to improve corrosion resistance and biocompatibility. Among various biomedical applications magnesium is widely studied on dental, orthopedic and vascular stent applications, recently. With different applications biodegradable magnesium implant not only need to control the corrosion rate but also enhance the functions according to the applications. In this study, magnesium structure has been controlled, and various bio-ceramic and bio-polymer were coated in different techniques according to the dental, orthopedic and vascular stent applications to enhance the function of the implants.

	Density (g/cm^3)	Compressive yield strength (MPa)	Elastic modulus (GPa)
Natural bone	**1.8-2.1**	**130-180**	**3-20**
Magnesium	**1.74-2.0**	**65-100**	**41-45**
Titanium	**4.4-4.5**	**758-1117**	**110-117**
Co-Cr	**8.3-9.2**	**450-1000**	**230**
Stainless steel	**7.9-8.1**	**170-310**	**189-205**

Table 1.1. Summary of the mechanical properties of various metal implant materials compared to natural human bone (Redrawn from ref [1])

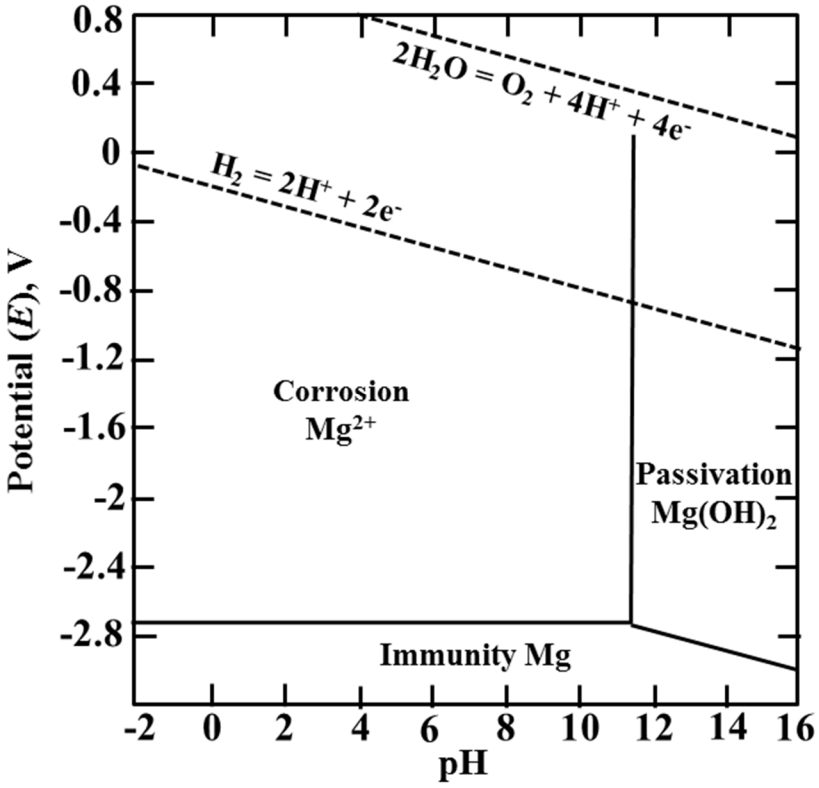

Figure 1.1. redox potential pH-value diagram for the Mg in water at 25 °C (Redrawn from ref [34])

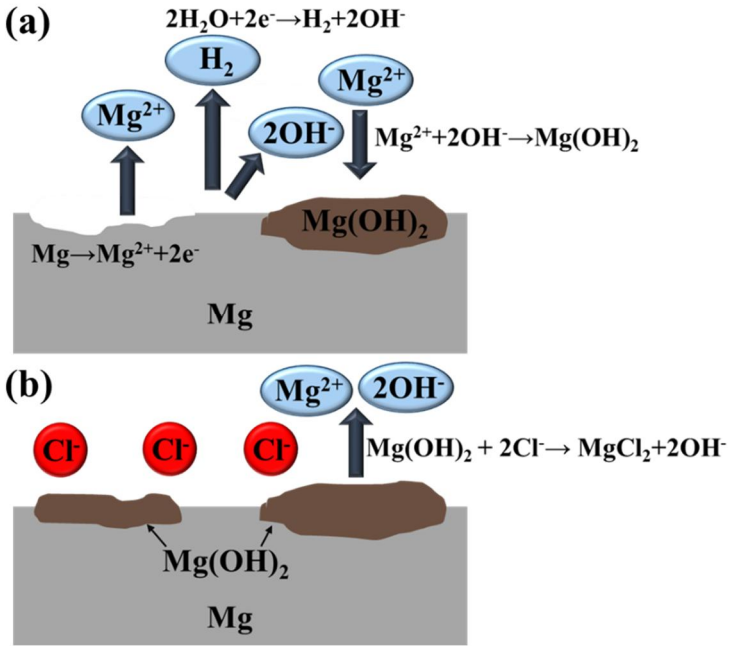

Figure 1.2. The schematic illustration of corrosion reactions of Mg in human body fluid. (a) the galvanic reaction between substrate and H_2O and (b) the decomposition of $Mg(OH)_2$ by Cl^- (Redrawn from ref [15])

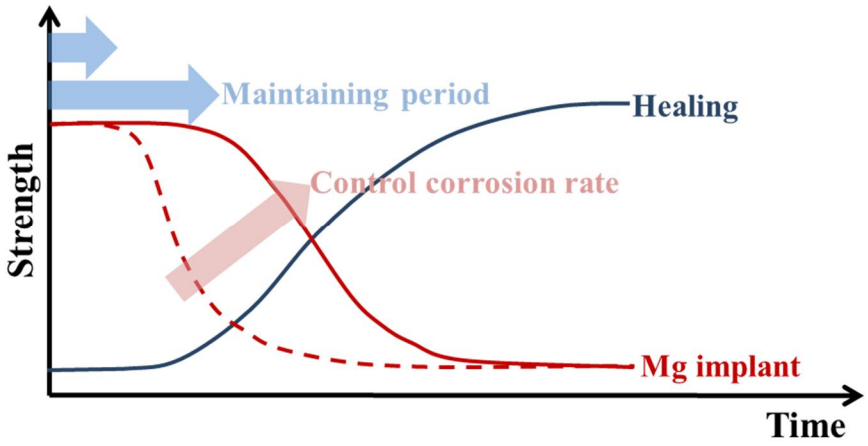

Figure 1.3. Ideal function of Mg implant in the human body by controlling the corrosion rate

Chapter 2.

PEI-Silica Hybrid Coating on Biomimetic HA Coated Porous Mg for Dental and Orthopedic Applications

2.1. Introduction

Metals have proven to be optimal materials for dental and orthopedic implants owing to their excellent strength and ductility, outperforming polymers and ceramics, especially in load bearing applications [35-38]. Titanium and its alloys, stainless steel, and cobalt–chromium alloys are widely used for bone fracture implants [39-42]. However, secondary surgery may be required after implantation of current metallic materials because of removal of implant after healing and adverse effects such as implant intolerance or loosening during prolonged healing, increasing health care costs, and patient discomfort [43-45]. As an alternative, biodegradable materials exhibiting sufficient mechanical stability and good biocompatibility have recently prompted much research interest.

Magnesium (Mg) and its alloys display good biocompatibility and mechanical properties closely approximating those of bone tissues, making them potential candidates for biomedical applications [1, 46-48]. Unlike their conventional metallic equivalents, magnesium implants do not require additional surgical removal owing to their biodegradability and bioresorbability [49, 50]. Moreover, many studies have suggested that porous scaffolds, in which pores promote bone ingrowth for firmer scaffold fixation and nutrient transport for better wound healing, are suitable for dental and

orthopedic applications [41, 51-54]. Therefore, magnesium scaffolds with a porous structure are potentially promising materials for medical implant applications.

However, one serious limitation in the use of porous Mg in medical implants is its excessively high corrosion rate. Not only does this fast bio-corrosion behavior deteriorate the mechanical strength of Mg implants, but it also leads to hydrogen gas evolution, which hinders cell attachment [1, 8, 55-57]. To inhibit corrosion of porous Mg, post-treatment is required, which may include surface treatment, alloying [1, 8, 55-57], or grain refinement [58]. Several studies have evaluated the effects of various Mg surface treatment methods, such as aerosol deposition, micro arc oxidation, fluoride treatment, and polymer coating [46, 50, 55, 59, 60], on the basis of degradation rates associated with different corrosion levels. Among these surface treatment methods, the hydroxyapatite (HA) coating through aqueous precipitation method was beneficial to coat complex shape of porous Mg with good corrosion resistance and biocompatibility with osteoblast cells [55-57].

In the previous research, HA coated porous Mg with different porosity (50-70%) has been fabricated [61]. However, the use of HA coated porous magnesium as a bone substitute under physiological conditions remains problematic. Porous magnesium structures in previous studies

demonstrated low strength and relatively fast corrosion rate in the human body [61-64]. Their applicability to implants require that their degradation rate not exceed the healing rate of the damaged tissue [65]. However, due to the inherent brittle performance of HA, cracks may form easily on HA coating layer during the deformation of the implant. Consequently, physiological fluid may penetrate through the cracks leading to the contact of the fluid with the Mg implant [66, 67]. Therefore, to successfully ensure the performance of load bearing Mg implants, a strategically designed porous magnesium scaffold with functional coating that simultaneously retains its excellent mechanical strength and corrodes at a controlled rate is necessary.

First, the mechanical properties of porous Mg scaffolds could be enhanced by mimicking the bone structure. Bone has combined dense and porous structure which may allow to have high strength and pore interconnectivity. By dense/porous combined structure of Mg scaffold as shown in Figure 2.1., Mg implant can have high strength while maintaining the advantages of porous structure. Therefore, in this study, we fabricated Mg mimicking the bone structure by spark plasma sintering process and space holder method.

Furthermore, the degradation rate of the biomimetic HA coated porous Mg scaffold can be decreased by dual coating the scaffold with

polymer to cover the cracks on HA coating layer. Poly(ether imide) (PEI) polymers can be a good candidate for dual coating material due to excellent adhesion strength to Mg, induced by its polar aromatic imide rings, in addition to its good flexibility and biocompatibility [46, 68-70]. Nevertheless, the concerns about low bioactivity of the PEI coating have yet to be resolved. PEI is less osteoconductive due to the low bioactivity compared to Mg implants coated with bio-ceramics such as HA. Thus, in this study, we proposed PEI-Silica hybrid materials as a dual coating layer on HA coated porous Mg, which allows the tunable corrosion behavior and enhanced biological behavior of the hybrid coated Mg by varying the amount of silica. The incorporation of silica into PEI may increase the corrosion rate of Mg through the reduced barrier properties or decreased hydrophobicity of the PEI coating [71, 72]. Moreover, excellent bioactivity of silica xerogels creates good chemical bonding with the surrounding bone tissues [71, 72].

Herein, biomimetic porous Mg, which was generated by subjecting Mg/NaCl composites to spark plasma sintering (SPS) and dissolving NaCl granules, was coated with a HA layer by aqueous precipitation coating process. Furthermore, PEI-Silica hybrid layer was dual coated on HA layer for the improvement of corrosion resistance and bioactivity. Structure and morphology of biomimetic HA coated porous Mg were examined by scanning

electron microscopy (SEM) and micro tomography (μ-CT). In addition, X-ray diffraction (XRD) characterization, and mechanical tests were conducted. Furthermore, the morphology, chemical composition, and hydrophilicity of HA/PEI-Silica hybrid coating layers were evaluated in terms of silica contents. In particular, the corrosion behavior of porous Mg coated with HA/PEI-Silica hybrids was carefully assessed under physiological conditions, and compared to HA coated porous Mg. The improved biological performance of hybrid coated Mg was also confirmed through *in-vitro* cell tests and *in-vivo* animal tests.

2.2. Experimental procedure

2.2.1. Fabrication of porous Mg

Mg powder (−100+200 mesh, Alfa Aesar, USA) and NaCl powder (+80 mesh, Sigma Aldrich, USA) were mixed with a small amount of ethanol as a binder. To fabricate porous Mg with different levels of porosity, the volume fraction of NaCl powder was varied (50%, 60% and 70%). The mixed powders were put inside a carbon die with 12 mm inner diameter and pressed with a load of 20 MPa inside an SPS (Well Tech, Korea) chamber. The sintering temperature was 585 °C. A holding time of 2 h and heating rate of 100 °C/min were employed during sintering. After densification by SPS, the sacrificial NaCl was dissolved in 1 M NaOH solution in vacuum desiccator [73]. The NaOH solution was exchanged periodically with ethanol as a buffer solution to prevent cracks and to rinse out the reaction products, such as $Mg(OH)_2$.

2.2.2. Fabrication of biomimetic porous Mg

Mg powder and NaCl powder were mixed with a small amount of ethanol. 70 vol% of NaCl powder was mixed with Mg powder to generate the high interconnectivity of the pores. Mixed powders were packed inside the

metal mold with different diameters (8 mm or 10 mm). 1 ton was pressed for 5 min to compact Mg/NaCl mixed powders. Compacted powders were put in the center of carbon die with 12 mm inner diameter. Pure Mg powder was put around the compacted powders. Sintering and dissolving NaCl were performed in similar process as fabricating porous Mg as shown in Figure 2.2.

2.2.3. HA/PEI-Silica hybrid coating

For HA coating on porous Mg, an aqueous solution was prepared by dissolving ethylenediaminetetraacetic acid calcium disodium salt hydrate (Ca (EDTA), Sigma Aldrich, USA) and potassium phosphate monobasic (KH_2PO_4, Sigma Aldrich, USA) in distilled water to obtain concentrations of 0.25 mol/L each. The pH level of the solution was adjusted to 8.9 with NaOH solution, and the solution was heated to 90 °C inside a vacuum oven [56, 57]. To form an HA coating layer on the surface, the porous Mg was immersed in the solution for 3 h.

Additionally, PEI-Silica hybrid layer was dual coated on HA coating layer. PEI solution was prepared by dissolving PEI pellets (Sigma Aldrich, USA) in 1-Methyl-2pyrrolidinone (NMP, Sigma Aldrich, USA) solvent by 15 w/v%. In addition, for the reagent of silica sol, tetramethylorthosilane (TMOS, Sigma Aldrich, USA), distilled water, hydrochloric acid (1N, HCl, Alfa Aesar,

USA), and NMP were mixed at a volume ratio of 5 : 1 : 0.02 : 3. The NMP was added after the reaction of silica sol to prohibit phase separation between the PEI solution and silica sol during the preparation of the PEI-Silica hybrid solution. Silica sol was mixed with PEI solution at 15, 30, and 45 volume ratio of silica. PEI-Silica hybrid coating with 15, 30, and 45 vol% will be referred to as PEI-15% Silica, PEI-30% Silica, and PEI-45% Silica. At over 45 vol% of silica, phase separation occurred while mixing the PEI solution and silica sol. Every solution was mixed in an oven at 37 °C to maintain the same mixing condition. After hybridization, HA coated porous Mg was immersed in each solution in vacuum desiccator. Solutions were put in the vacuum desiccator to immerse the solution inside the pores effectively. After coating process, specimens were dried in 70 °C dry oven for the dense PEI-Silica hybrid coating layer with perfect evaporation of NMP. Scheme of the HA aqueous precipitation coating on porous Mg and PEI-Silica hybrid coating on HA coated porous Mg are shown in Figure 2.3.

2.2.4. Characterization of Mg scaffold

Microstructure and 3D structure were observed by SEM (JSM 6360, JEOL, Japan) and μ-CT (Skyscan 1173, Kontich, Belgium). Microtomography images were acquired at a resolution of 10 μm using a 1.0 mm aluminum filter.

The μ-CT scanner operated at 90 kV and 88 μA. The approximate porosity was calculated using measured mass (m_S) and volume (V_S)

$$p\ (\%) = 100\left(\frac{{}^{ms}/_{Vs}}{\rho Mg}\right) \quad (1)$$

where p is the total porosity in percentage, m_S / V_S is the measured density and ρMg is the theoretical density of the Mg.

Furthermore, porosity and pore size were also evaluated by processing the acquired μ-CT images using CTAn (Skyscan, Kontich, Belgium).

The phase analyses were performed by X-ray diffraction (XRD, D8-Advance, BRUKER, Germany) with Cu Kα source and the scanning speed of 1°/min.

2.2.5. Mechanical behavior of Mg scaffold

The mechanical properties of the fabricated Mg scaffolds were measured using an Instron 5582 System (Instron, Norwood, USA) under a displacement-controlled mode, with a cross-head speed of 1 mm/min. The four specimens used to examine the compressive strengths were 12 mm in diameter and 6 mm in height.

2.2.6. Characterization of HA/PEI-Silica hybrid coating

The surface morphology and thickness of the HA, or HA/PEI or HA/PEI-Silica hybrid coating layers on porous Mg were observed by field-emission scanning electron microscopy (FE-SEM, SUPRA 55VP, Carl Zeiss, Germany) and focused ion beam (FIB, AURIGA, Carl Zeiss, Germany) respectively. The distribution and the particle size of the silica were observed with a transmission electron microscope (TEM, JEM-2100F, JEOL, Japan). To observe the particles with TEM, PEI-Silica hybrid the solution was spin-coated on the copper grid (400 mesh, TED PELLA Inc., USA). The chemical structures of the hybrid coating layers were evaluated by Fourier transform infrared spectroscopy (FT-IR, Nicolet 6700, Thermo Scientific, USA). Moreover, the hydrophilicity of the coating layers was examined by observing the contact angle of the distilled water droplet using the Phoenix 300 contact angle analyzer (surface Electro Optics Co. Ltd, Korea). Six specimens were tested for each coating condition.

2.2.7. *In-vitro* corrosion behavior evaluation

The corrosion behavior was evaluated by monitoring the amount of

hydrogen gas evolved after immersing bare porous Mg or HA, HA/PEI or HA/PEI-Silica hybrid (15 and 30 vol%) coated porous Mg in 80 ml of simulated body fluid (SBF) at 37 °C. The specimens were in a diameter of 12 mm and a thickness of 1.5 mm. Three specimens were tested for each condition. The SBF was prepared using the method proposed by Kokubo et al [74].

2.2.8. *In-vitro* biological behavior evaluation

The initial cell adhesion of the pre-osteoblast cell (MC3T3-E1, ATCC, CRL-2593, USA) was performed. Every specimen was cleansed in 70% ethanol and dried for 24 hours in a vacuum chamber. After drying the specimens, they were placed on a clean bench for 1 hour for sterilization with ultraviolet light. The cells were cultured in an alpha minimum essential medium (α-MEM, Welgene, USA) supplemented with 5% fetal bovine serum (FBS, Gibco, USA) and 1% penicillin-streptomycin (Pen strep, Gibco, USA) in a humid incubator with 5% CO_2 at 37 °C.

The initial cell attachment was observed with SEM after 6 hours of cell seeding with the density of 5×10^4 cells/ml on HA or HA/PEI-Silica (0, 15 or 30 vol%) hybrid coated porous Mg. The SEM specimens were prepared by immersing in 2.5% glutaraldehyde (Sigma Aldrich, USA) for 10 min,

dehydrating in graded ethanol (70, 90, 95, and 100% ethanol in sequence) and finally immersing in hexamethyldisilazane (Sigma Aldrich, USA) for 10 min.

2.2.9. *In-vivo* biodegradation and bone response evaluation

New Zealand white rabbits (3-month-old males weighing 3.0–3.5 kg) (Kosabio, Korea) were used to evaluate the *in-vivo* biodegradation and bone response of the HA, HA/PEI or HA/PEI-15% Silica coated biomimetic porous Mg. *In-vivo* animal experiment was conducted using the rabbit femoropatellar groove model in accordance with the procedure reported in the literature [75]. All rabbits were anesthetized through intramuscular injection of a combination of 0.1 mL of 2% Xylazine HCl (Rompun, Bayer Korea, Korea), 0.2 mL of Tiletamine HCl (Zoletil, Virbac Laboratories, France), and Lidocaine (Yuhan Corporation, Korea). After anesthetization the patella was dislocated laterally and the surface of the femoropatellar groove was exposed. A full-thickness cylindrical cartilage defect (5 mm in diameter, 4 mm in depth) was created in the patellar groove. The HA, HA/PEI or HA/PEI-15% Silica coated biomimetic porous Mg which had similar structure of the natural bone were implanted in the cartilage defects as shown in Figure 3.4.

At 5 weeks after the implantation, the rabbits were sacrificed to

extract the regions of bone defect. To evaluate new bone formation, the harvested bone tissues were scanned by μ-CT with 1.0 mm aluminum filter at a resolution of 17 μm, a voltage of 90 kV and a current of 88 μA. The cross section images of the specimens and bone tissues were obtained using post processing software (Data Viewer 1.4). The bone regeneration volume was evaluated by processing the acquired μ-CT images using CTAn. Three specimens were examined to obtain the mean value and standard deviation.

2.2.10. Statistical analysis

All data are expressed as mean ± standard deviation (SD). The statistical analysis was performed by one-way analysis of variance with Bonferroni's post-hoc comparison. A p value inferior to 0.05 was considered statistically significant in all cases.

2.3. Results and discussion

2.3.1. Physical and chemical structure of porous Mg

Figure 2.5. shows the typical optical image of porous Mg with different porosities (50%, 60% and 70% porosity). The porosity of Mg was well controlled by volume contents of NaCl. No signs of carbonization were observed after the SPS and pore generating process. This suggests that SPS and space holder method are effective to fabricate porous Mg scaffolds with various porosities. However, porosity of Mg scaffold was limited from 50 to 70% due to the shape of the pore generator and the mechanical strength of Mg. It should be noted that as the porosity decreases lower than 50% the amount of NaCl which is not eliminated during the pore generating process increases. Moreover, the porous Mg with porosity higher than 70% had thin Mg struts which results in low mechanical strength.

Figure 2.6. shows the SEM images of the porous Mg scaffolds with various porosities (70, 60, and 50 vol.%). The Mg scaffolds showed large pores with good pore interconnectivity, while Mg particles were fully densified without any noticeable pores or defects, showing that SPS allowed for the achievement of full densification of Mg walls, which would be hardly obtainable using conventional techniques to fabricate porous Mg [62, 64, 76-

79].

A cross-sectional μ-CT image of the specimens showed a uniform distribution of pores with high pore interconnectivity shown as Figure 2.7. White dots indicate NaCl remained after pore generating process. Amount of the remained NaCl increased as the porosity decreased due to the increase of the closed pores. The porosity and the pore sizes of each specimen were calculated using the program and provided a calculated porosity similar with the porosity according to Eq. (1). The pore size of the specimens was 240 μm in average, indicating their suitability for osteoconduction upon implantation [80, 81].

Figure 2.8. shows the XRD patterns of Mg/NaCl composite with 60 vol% of NaCl after sintering and porous Mg after dissolving NaCl. XRD patterns mainly displayed peaks corresponding to Mg and NaCl for Mg/NaCl composite but not NaCl peaks for porous Mg. This suggests that NaCl particles were properly removed in the presence of NaOH [73]. Moreover, dominant peaks of oxidized or carbonized Mg were not found on the XRD pattern, indicating the oxidation or carbonization which occurs easily during general sintering process did not occur during SPS.

2.3.2. Mechanical behaviors of porous Mg

The mechanical properties of the bare porous Mg with different porosities (50%, 60% and 70%) were evaluated by compression tests. Typical stress–strain diagrams for the porous Mg specimens with various porosities are shown in Figure 2.9. All porous specimens produced exhibited ductile behavior under compression, demonstrating the suitability of the SPS technique for densifying Mg compacts without the oxidation and carbonization of Mg powders. Figure 2.10. shows the average ultimate compressive strength and stiffness of the porous Mg with various levels of porosity (50%, 60% and 70%). The average ultimate compressive strengths of porous Mg with 50%, 60% and 70% porosity were 30 MPa, 15 MPa and 7 MPa, respectively, and the average elastic modulus were 0.49 GPa, 0.33 GPa, and 0.23 GPa, respectively. These values are compatible with those for human cancellous bone [1] and comparable with those reported in the literature [62, 64].

2.3.3. Physical structure of biomimetic porous Mg

Figure 2.11. shows the typical optical image of biomimetic porous Mg with different ratio of dense/porous structure, resulting in different total porosity (70%, 49% and 31% porosity). The ratio of dense/porous structure

was controlled by controlling the volume of Mg/NaCl compact before sintering. 70% porosity was selected for the porous structure for the high interconnectivity of the pores. The final structure was hierarchical, with two different dense and porous structure, resembling the structure of a bone [82-84].

Figure 2.12. shows the SEM images of the interface of dense/porous structure, and high magnification of each dense and porous structure of the biomimetic porous Mg. From the low magnification, porous structure had large pores with good pore interconnectivity similar with that of the porous Mg with 70% porosity. Moreover, the interface between the two structures remained intact during the sintering step. By high magnification of each dense and porous structure, it was found that Mg particles were fully densified without any noticeable pores or defects by SPS.

A cross-sectional μ-CT image of the specimens showed a uniform distribution of pores with high interconnectivity as shown in Figure 2.13. Moreover, cross-sectional images and 3D reconstructed images showed similar structure of biomimetic porous Mg with that of the natural bone. The porosity and the pore sizes of each specimen were calculated using the program and the total porosity of the Mg scaffold had similar with the porosity according to Eq. (1). Furthermore, porous structure had average pore

size of 240 μm similar with the porous Mg due to the same size of NaCl space holder.

2.3.4. Mechanical behaviors of biomimetic porous Mg

The compressive stress-strain curve and compressive mechanical behaviors of the biomimetic porous Mg with different ratio of the dense/porous structure were evaluated (Figure 2.14. and Figure 2.15.). The ultimate compressive strength and stiffness of biomimetic porous Mg with 70%, 49% and 31% porosity were 4 MPa, 15MPa and 71 MPa, and 0.13 GPa, 0.42 GPa and 0.67 GPa respectively. The enhanced compressive strength was mainly attributed to the increase in the portion of the dense structure. By controlling the dense/porous ratios of the scaffolds, the structural and compressive features can be customized to match those of the surrounding bones at the implant site [85, 86]. The compressive strengths of fabricated biomimetic porous Mg scaffolds with bone-like structures were within the range of 15–70 MPa, which are in the range of those in tibia, femur, and trabecular bone, with or without marrow [86, 87].

2.3.5. Morphology and chemical structure of HA/PEI-

Silica coating layers

A dense HA layer comprised of needle-shaped HA crystals with a thickness of ~2 μm of was formed uniformly on the surfaces of porous Mg (Figure 2.16. (a, f)) [61]. In addition, surface morphologies of pure PEI and PEI-Silica hybrid coating layers which were dual coated on HA layer are shown in Figures 2.16. (b)–(e). The pure PEI, PEI-15% Silica, and PEI-30% Silica hybrid coating layers were found to cover the HA coating layer homogenously. On the other hand, on the surface of the PEI-45% Silica coating layer, a small number of cracks appeared occasionally (Figure 2.16. (e)). The hybrid coating layer with silica >45 vol% was found to have the greater number of cracks as the silica content increased, failing to cover the entire Mg surface [88]. The representative cross-section image of HA/PEI-Silica hybrid coated porous Mg is shown in Figure 2.16. (f). Some of the cracks were found on the HA layer propagating to the surface of porous Mg. However, dense PEI-Silica hybrid layer was completely covering the cracks of HA coating layer. Even though the viscosity of hybrid sols had decreased with the increased amount of silica sol, the coating thickness of the PEI or PEI-Silica layers was almost identical under the current dip coating and drying conditions. Moreover, the vacuum state during the dip coating allowed the good infiltration of pure PEI or PEI-Silica into the nano-roughened HA

surface. Due to the nanoscale roughness of HA, interfacial surface area between HA and polymer increased resulting in a strong bonding between two layers.

The high resolution TEM image and EDS pattern in Figure 2.17. show the silica nanoparticles embedded in the PEI matrix for PEI-15% Silica. The size of silica nanoparticles was 50–300 nm and the degree of agglomeration was low, avoiding prominent clusters. Therefore, it was confirmed that the sol–gel method could produce homogeneous PEI-Silica hybrid systems with minimal agglomeration of the silica phase. Above 45 vol% of silica, the PEI-Silica coating layers became brittle due to the relatively large contents of silica [71]. Therefore, during the drying process, the solidified hybrid coating layer with higher silica contents (>45 vol%), in which the silica phase became dominant in the hybrid systems, contained significant surface cracks due to induced stresses within the coating layer, often caused by the volume contraction of the coating constrained by the underneath substrate [89]. Therefore, in this study, PEI-15% Silica and PEI-30 vol% Silica were chosen for crack-free and homogeneous hybrid coating layers on HA layer, after comparison with the pure PEI coating.

Figure 2.18. shows the FT-IR spectrum of pure PEI or PEI-Silica hybrid (15 and 30 vol %) coating layers on Mg. Main peaks at 1778 and 1720

cm^{-1} were detected, corresponding to the symmetric and asymmetric stretching vibration of C = O groups. The peak at 1353 cm^{-1} was related to the symmetric stretching of C–N–C in the imide ring [46]. Moreover, the 900–1200 cm^{-1} peaks indicated overlapping of the asymmetric stretching vibrations of the siloxane groups (Si–O–Si) and silanol groups (Si–OH) [90]. In the case of the PEI-Silica hybrids, the intensity of the 900–1200 cm^{-1} peaks became stronger as the silica content increased because of the larger amount of silica bonding. Besides the PEI or silica-related characteristic peaks, no significant peaks were observed, implying that the PEI and silica maintained their inherent properties without any significant deterioration due to the undesirable reactions between PEI and silica.

2.3.6. Hydrophilicity of HA/PEI-Silica coating layers

Hydrophilic materials have previously been incorporated with a relatively hydrophobic polymer matrix in order to improve the hydrophilicity of the matrix for enhanced biodegradability and better cell affinity of coated Mg [71, 72, 91]. Thus, the contact angle was measured to observe the silica influence on wettability of PEI as shown in Figure 2.19. The HA coated Mg was highly hydrophilic showing the contact angle nearly 0°. HA has large amount of hydroxyl functional groups resulting in highly hydrophilic [92].

After dual coating with pure PEI, contact angle increased about to 65°. As the amount of silica increased from 15 vol% to 30 vol%, the equilibrium contact angle gradually decreased from about 58° to about 52°, and the water droplet on the surface of hybrid coating layers became more spread as the silica content increased. Therefore, the incorporation of silica clearly improved hydrophilicity of PEI-Silica hybrid coatings.

2.3.7. *In-vitro* corrosion behavior of HA/PEI-Silica coated porous Mg

Corrosion tests with porous Mg specimens coated with HA, HA/PEI and HA/PEI-Silica (15 and 30 vol% silica) were performed by immersing these specimens in SBF, compared to bare porous Mg (Figure 2.20.). One of the major outcomes from the corrosion reaction of Mg (H_2 gas generation), were monitored as indicators of Mg corrosion. Bare Mg corroded the most rapidly, generating the highest volume of hydrogen gas, whereas coating on porous Mg decreased the corrosion rate of porous Mg. However, by dual coating pure PEI or PEI-Silica hybrid on HA layer further decreased the corrosion rate and increasing the stability of the porous Mg. PEI dual coated porous Mg corroded the least with a minimal generation of H_2 gas generation. The corrosion behavior of the hybrid coated Mg fell between that of HA

coated porous Mg and HA/PEI dual coated porous Mg, varying with the amount of incorporated silica. The removal of silica through the dissolution process in SBF might create nano-sized voids within the PEI matrix which, in return, were filled with water, creating the penetration path of water to the underneath porous Mg. The incorporation of silica nanoparticles in the PEI coating clearly increased the corrosion rate of Mg substrate underneath the coating layer. Zomorodian et al [93] also found that HA nanoparticles in the PEI coating decreased the corrosion resistance of Mg alloys due to the decreased pore resistance in the coating layer. The increased porosity of the coating layer can likely be attributed to the fast dissolution of the silica nanoparticles. Moreover, the number of pores controlled by the silica content positively correlated with the corrosion rate of Mg. Furthermore, the improved hydrophilicity of the PEI coating due to silica might contribute to the increased corrosion rate of Mg. The improved water accessibility to the relatively hydrophilic surface of hybrid coating could enhance the diffusion of water through the coating layer, compared to the pure PEI coating surface. However, all pure and hybrid dual coatings were found to significantly reduce the released volume of H_2 gas generated from porous Mg compared to HA coated porous Mg (Figure 2.20.), showing the good corrosion resistance by dual coating.

2.3.8. *In-vitro* biological behavior of HA/PEI-Silica coated porous Mg

The initial cell morphology on the HA/PEI-Silica hybrid coated Mg were evaluated and compared to the both HA coated porous Mg and HA/PEI coated porous Mg. Figures 2.21. shows the early-stage morphology of the MC3T3-E1 cells after 24 h cell culturing on porous Mg specimens coated with HA, HA/PEI or HA/PEI-Silica hybrid (15 and 30 vol%). On the HA coated porous Mg, only a few cells were attached, with an almost round shape with minimal spreading (Figures 2.21. (a)). The poor cell attachment of HA coated porous Mg has been attributed to the rapid pH increase and H_2 evolution during corrosion [29, 50, 93]. However, the cells were strongly attached to the HA/PEI and HA/PEI-Silica coated porous Mg surfaces as shown in Figures 2.21. (b)-(d). Importantly, the cells became more spread out and flattened on the HA/PEI-Silica hybrid coating layer than those on the HA/PEI coating layer. The relatively hydrophilic character of hybrid coating likely improved the cell affinity of the surface, promoting cell attachment at the early stage of cell growth, besides the effect of the released Mg and Si ions from the corroded Mg [71, 72, 88, 91]. The *in-vitro* cell tests clearly demonstrated that PEI-Silica hybrid coating layers could enhance the

biological performance of the HA coated porous Mg implants compared to the PEI coating, mainly due to the increased hydrophilicity and amount of Mg and Si ions. It is known that the appropriate amount of Mg or Si ions can improve cell attachment, proliferation, and differentiation [71, 94, 95].

2.3.9. *In-vivo* biodegradation and bone response

HA, HA/PEI or HA/PEI-15% Silica coated biomimetic porous Mg which had similar structure with that of the natural bone were implanted into rabbit femoropatellar defects to closely evaluate their bone responses. After 5 weeks of healing, the specimens and surrounding bone tissues were extracted as shown in Figure 2.22. New tissues formed on the top of the HA/PEI-15% Silica coated biomimetic porous whereas some of HA coated and HA/PEI coated specimen were not covered with the new tissues. The morphology of the implanted specimens and the new bone formation were observed with μ-CT. Figure 2.23. shows representative cross-sectional image of the specimens and surrounding bone tissues. The gray and white represent the Mg specimen and the original bone tissue regions, respectively. Specimens with different coatings exhibited different degradation rates. In the case of HA coated and HA/PEI-15% Silica coated specimen, corrosion occurred faster than HA/PEI coated specimen after 5 weeks of implantation showing some collapse of the

structure. This result had similar trend with the result of *in-vitro* corrosion test in Figure 2.20. However, the HA/PEI-15% Silica coated specimen exhibited the better formation of new bone near the defect boundaries and bone ingrowth towards the inner part of the scaffolds to some extent. Furthermore, the new bone volume was measured by μ-CT analysis. Figure 2.24 shows the new bone volume formed inside the pores of the biomimetic Mg. Similar result with the cross-sectional μ-CT images, the HA/PEI-15% Silica coated specimen exhibited the higher volume of bone regeneration inside the pores of the specimen compared with HA, HA/PEI coated specimens. It can be stated that the HA/PEI-15% Silica coated biomimetic Mg showed the highest extent of bone ingrowth, which demonstrates the efficacy of HA/PEI-Silica hybrid coating as a means of decreasing the corrosion rate than HA coating and promoting bone regeneration than HA/PEI coating. These results are in agreement with earlier studies where a bioactive silica hybridized-coating layer was reported to promote bone-implant interaction and lead to a good contact with the surrounding bone tissue [96]. Improvement of bio-corrosion resistance, biocompatibility and bone response on biomimetic porous Mg achieved in this work through coating with HA/PEI-Silica gives promise for greater acceptance of Mg implants in biomedical industry.

2.4. Conclusions

In this study, we fabricated biomimetic porous Mg mimicking the structure of the bone by the spark plasma sintering of Mg powder blended with NaCl powder, which served as a sacrificial space holder. The biomimetic porous Mg obtained after the dissolution of the NaCl particles possessed good mechanical properties and a pore structure with high interconnectivity of the pores that qualifies the materials for applications in dental and orthopedic implants. Furthermore, the bio-corrosion of porous Mg was significantly inhibited by HA/PEI-Silica coating. HA coating decreased corrosion rate of porous Mg, however, due to the brittle characteristic of HA, cracks formed on the coating layer and acted critically to the corrosion of porous Mg. As a result, homogeneous PEI-Silica hybrid materials were successfully fabricated with various silica contents using the sol–gel method, and were dual coated on HA coated porous Mg by dip coating process. The 50–300 nm sized silica nanoparticles were well dispersed in the PEI matrix without significant particle agglomeration up the 30 vol% silica. The corrosion rate remarkably decreased by dual coating pure PEI or PEI-Silica hybrid on HA coated porous Mg compared with bare and HA coated porous Mg. Moreover, the biocompatibility of the HA/PEI-Silica hybrid coated porous Mg specimens were significantly improved, mainly due to the higher hydrophilicity and Mg

and Si ion concentrations associated with faster corrosion compared to the HA/PEI dual coated porous Mg. Therefore, PEI-Silica hybrid systems have considerable potential as a coating material of Mg for dental and orthopedic applications by providing enhanced corrosion resistance and biological performance.

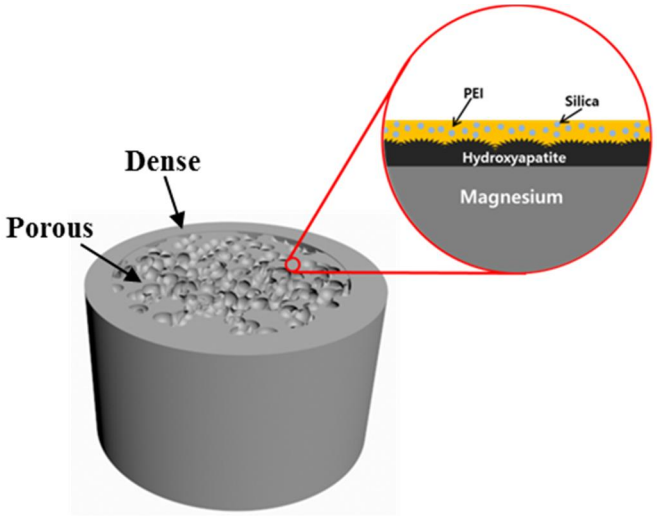

Figure 2.1. Scheme of the structure and coating layer of PEI-Silica dual coated biomimetic Mg

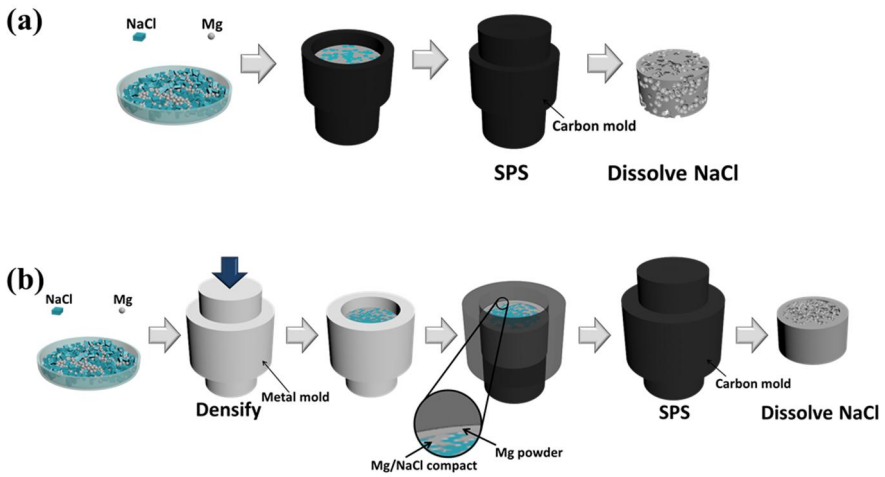

Figure 2.2. Experimental procedure of fabricating Mg with (a) porous structure and (b) biomimetic structure

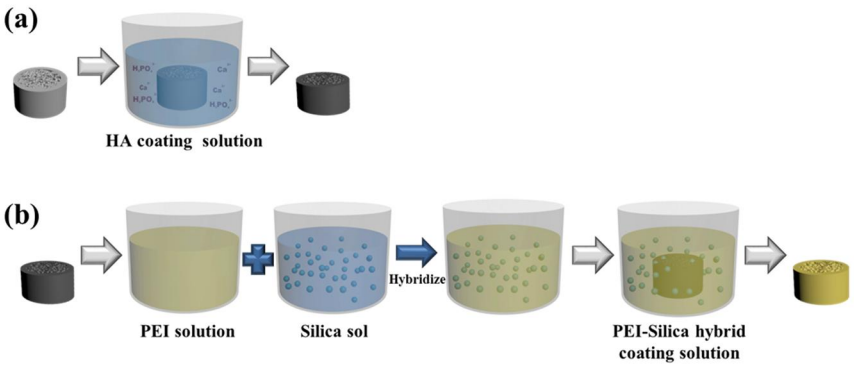

Figure 2.3. Experimental procedure of (a) aqueous precipitation coating of HA on porous Mg and (b) dip coating PEI-Silica hybrid on HA coated porous Mg by sol-gel method

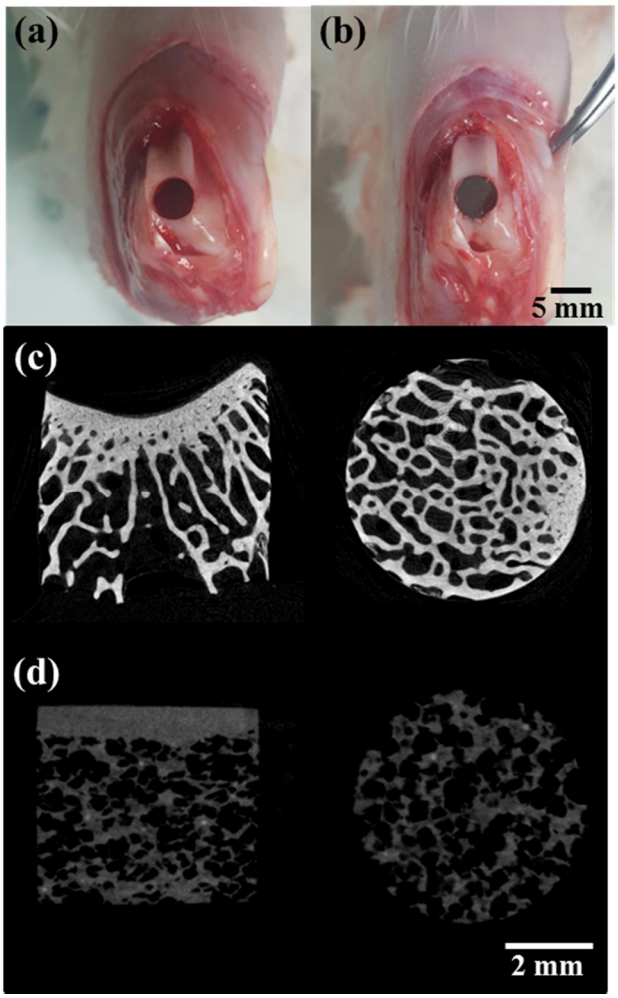

Figure 2.4. *In-vivo* rabbit femoropatellar groove model experiment (a) before implantation and (b) after implantation of biomimetic porous Mg; cross sectional μ-CT image of (c) natural femoropatellar bone and (d) biomimetic porous Mg

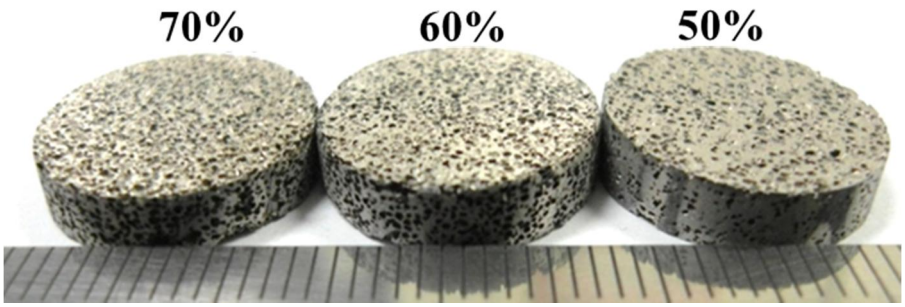

Figure 2.5. Optical images of porous Mg with 70%, 60%, and 50% porosity fabricated by SPS and space holder method

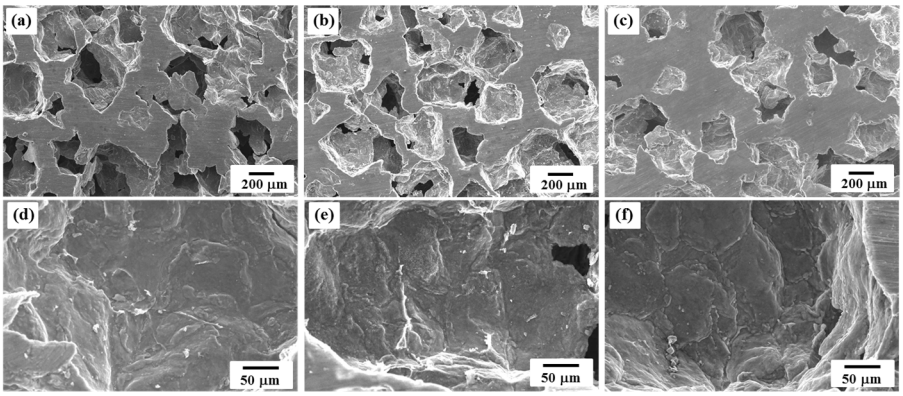

Figure 2.6. SEM images of porous Mg with (a. d) 70%, (b. e) 60%, and (c, f) 50% porosity in low and high magnification respectively

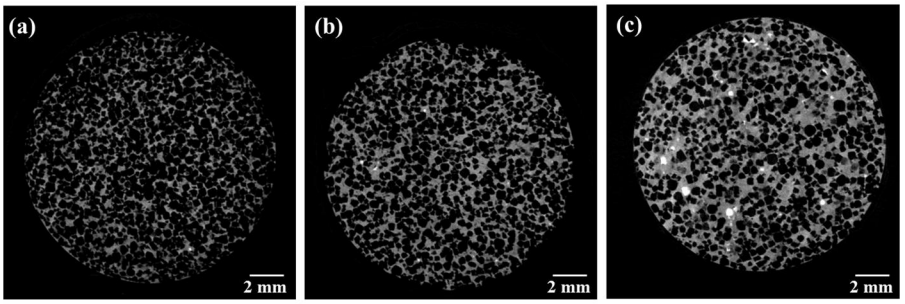

Figure 2.7. Cross sectional μ-CT images of porous Mg with (a) 70%, (b) 60%, and (c) 50% porosity

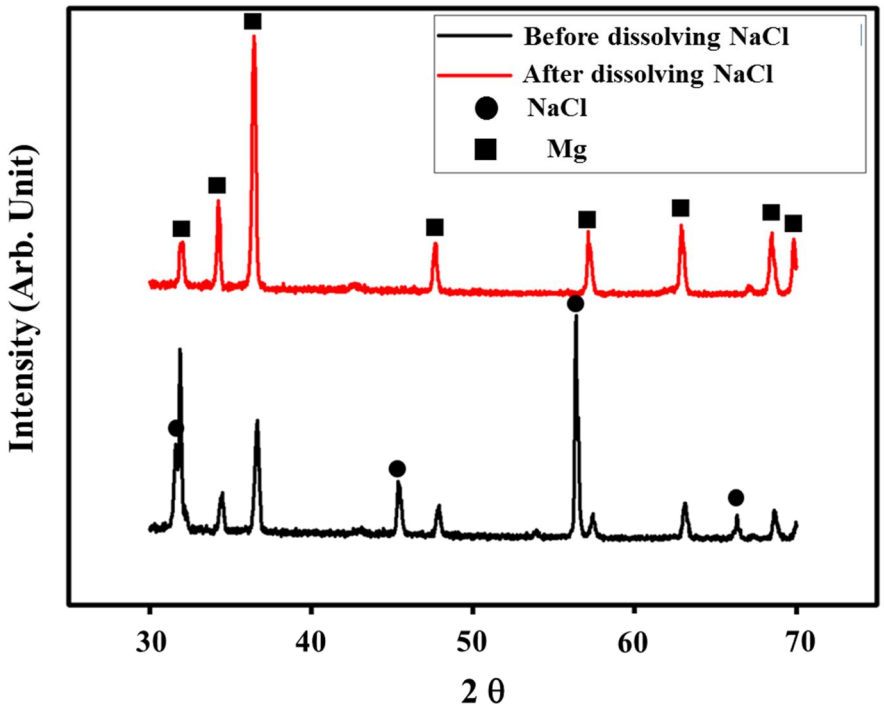

Figure 2.8. XRD patterns of Mg/NaCl composite after SPS and after dissolving NaCl

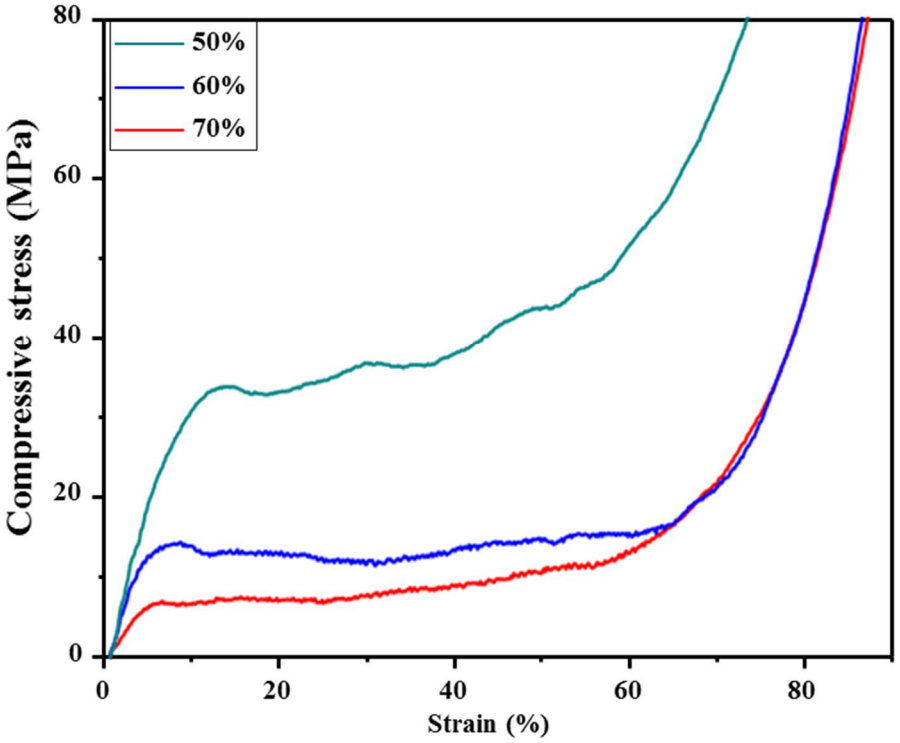

Figure 2.9. Stress-strain curve of porous Mg with different porosity (50%, 60%, and 70%)

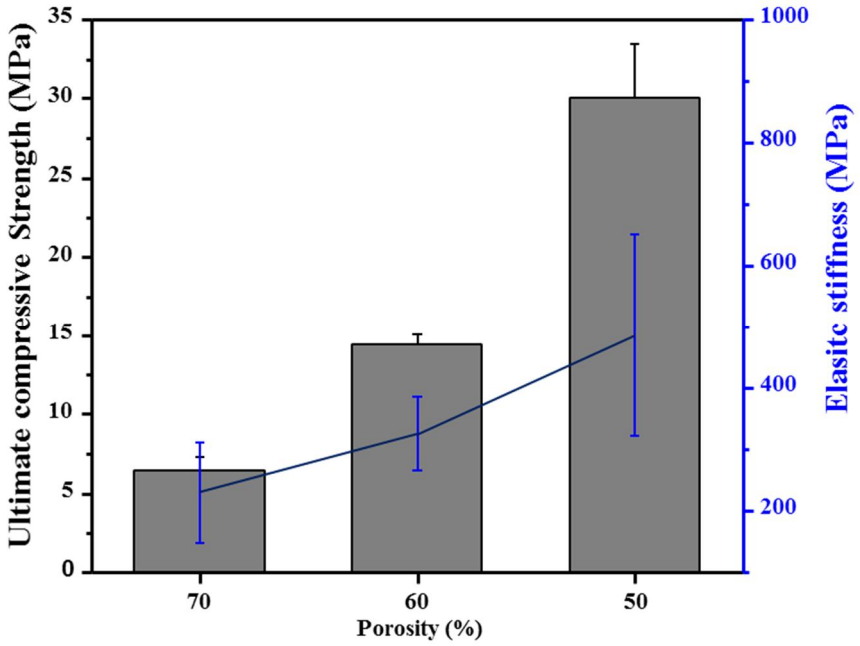

Figure 2.10. Ultimate compressive strength and stiffness of porous Mg with different porosity (50%, 60%, and 70%)

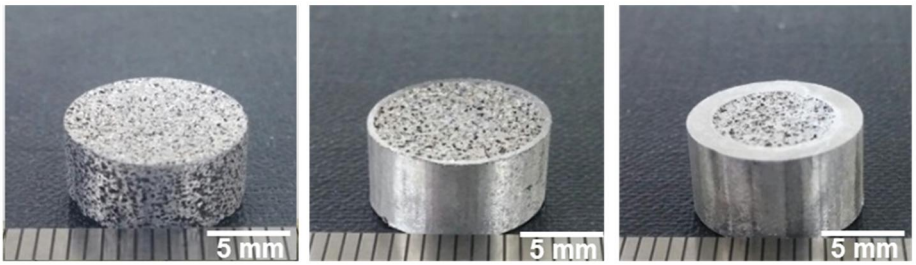

Figure 2.11. Optical images of biomimetic porous Mg with (a) 70%, (b) 49%, and (c) 31% porosity

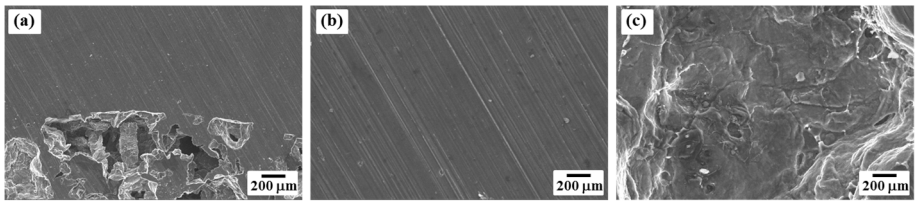

Figure 2.12. SEM images of (a) interface of dense/porous structure, and high magnification of (b) dense structure and (c) porous structure of biomimetic porous Mg

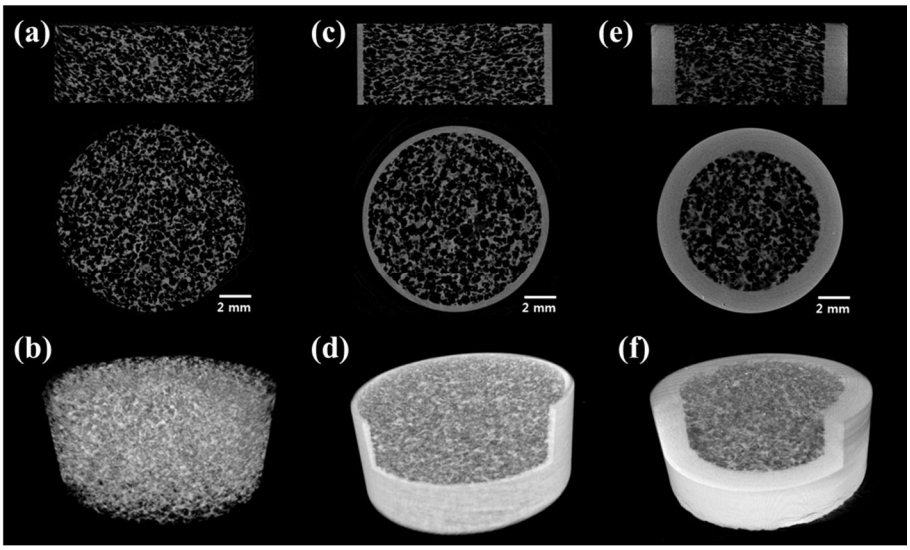

Figure 2.13. Cross sectional μ-CT images of biomimetic porous Mg with (a) 70%, (c) 49%, and (e) 31% porosity and 3D reconstructed structure of biomimetic porous Mg with (b) 70%, (d) 49%, and (f) 31% porosity

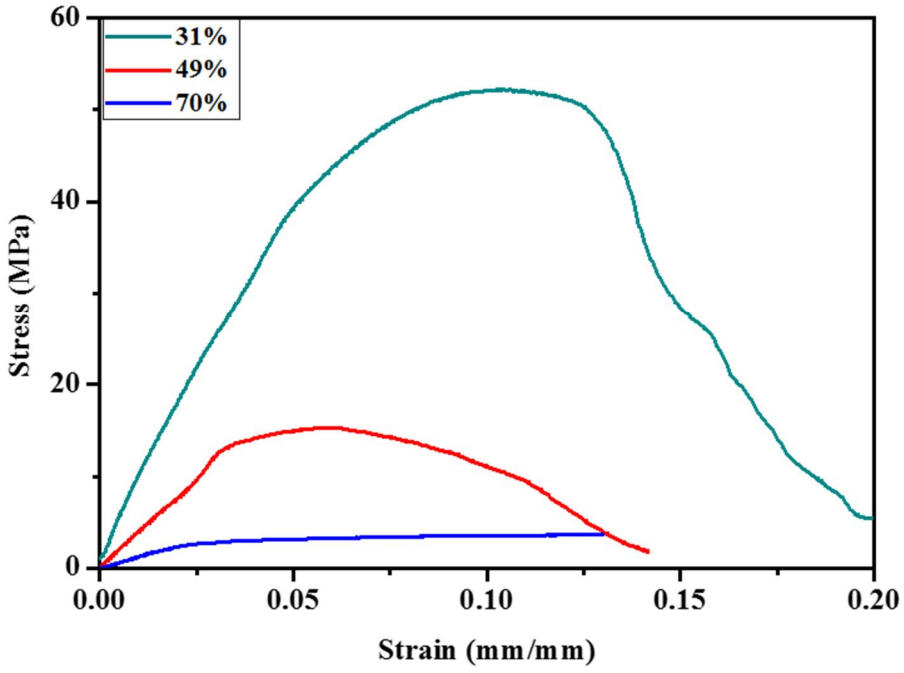

Figure 2.14. Stress-strain curve of biomimetic porous Mg with different porosity (31%, 49%, and 70%)

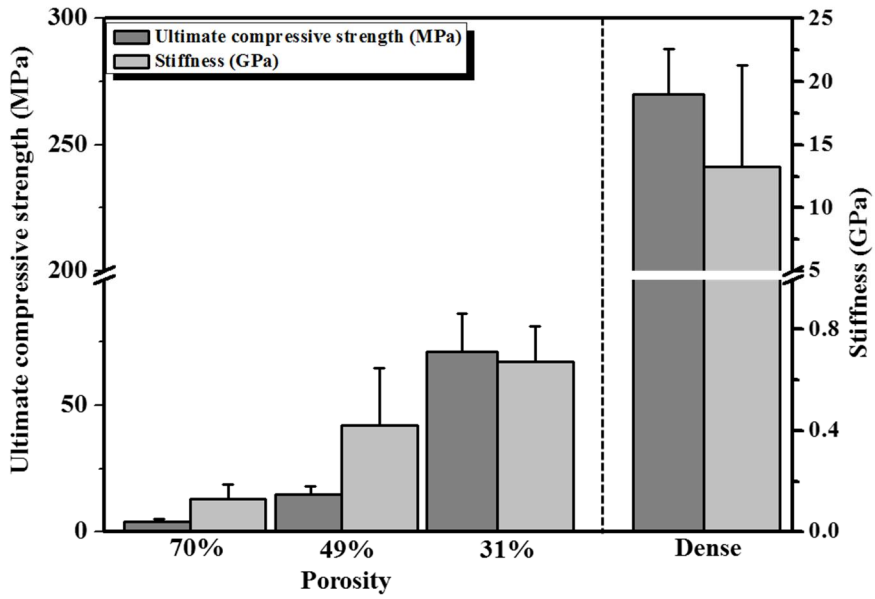

Figure 2.15. Ultimate compressive strength and stiffness of biomimetic porous Mg with different porosity (31%, 49%, and 70%) and dense bulk Mg

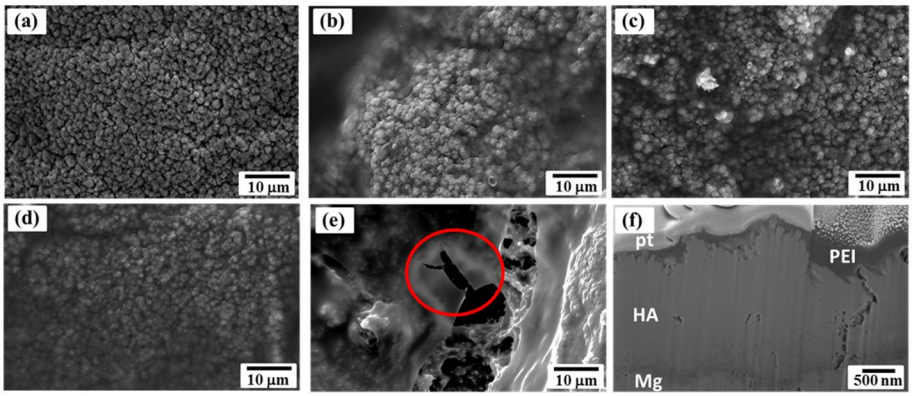

Figure 2.16. Surface SEM images of (a) HA, (b) HA/PEI-0% Silica, (c) HA/PEI-15% Silica, (d) HA/PEI-30% Silica and (e) HA/PEI-45% Silica coated porous Mg, and cross sectional image of (f) HA/PEI-15% Silica coated porous Mg

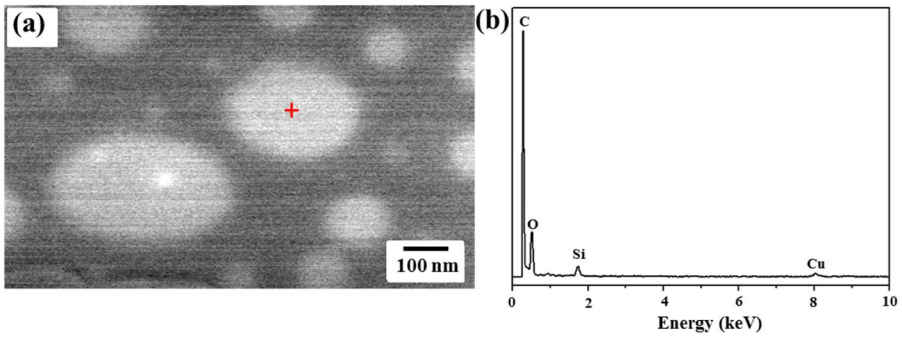

Figure 2.17. (a) TEM image, and (b) EDS patterns of silica nano particles dispersed in PEI matrix

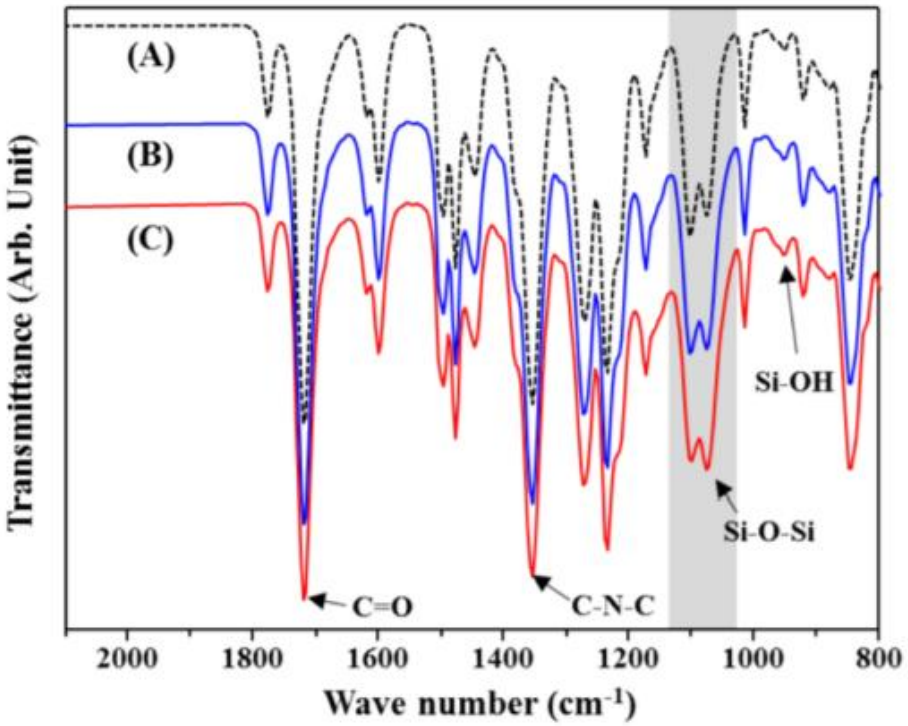

Figure 2.18. FT-IR transmission spectrum of (A) pure PEI, (B) PEI-15% Silica and (C) PEI-30% Silica coating layers on Mg surface

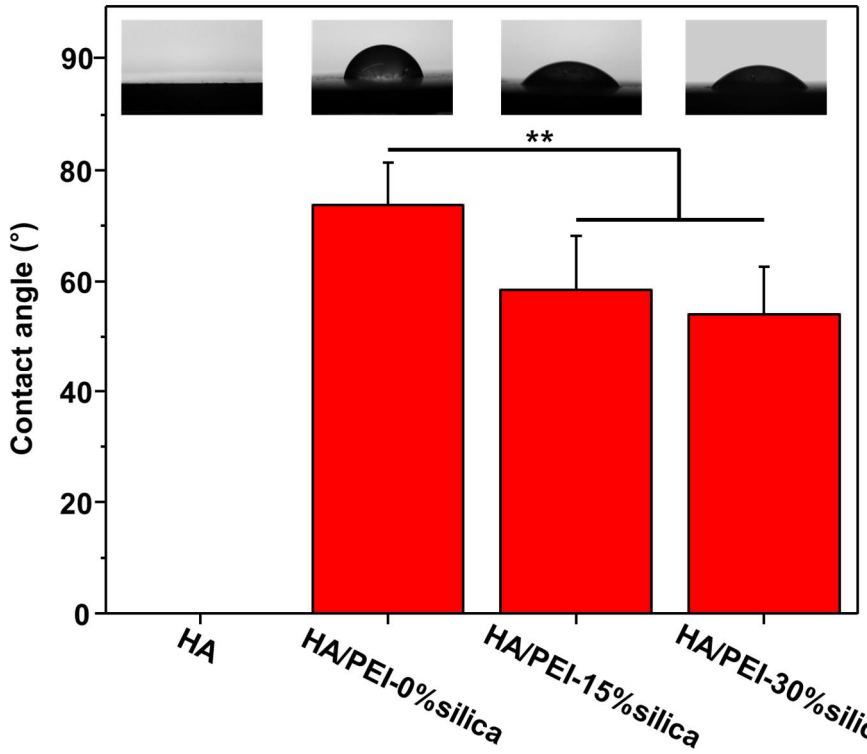

Figure 2.19. Water contact angle on HA, and HA/PEI-Silica (0 vol%, 15 vol% and 30 vol%) dual coated Mg (**$p < 0.005$)

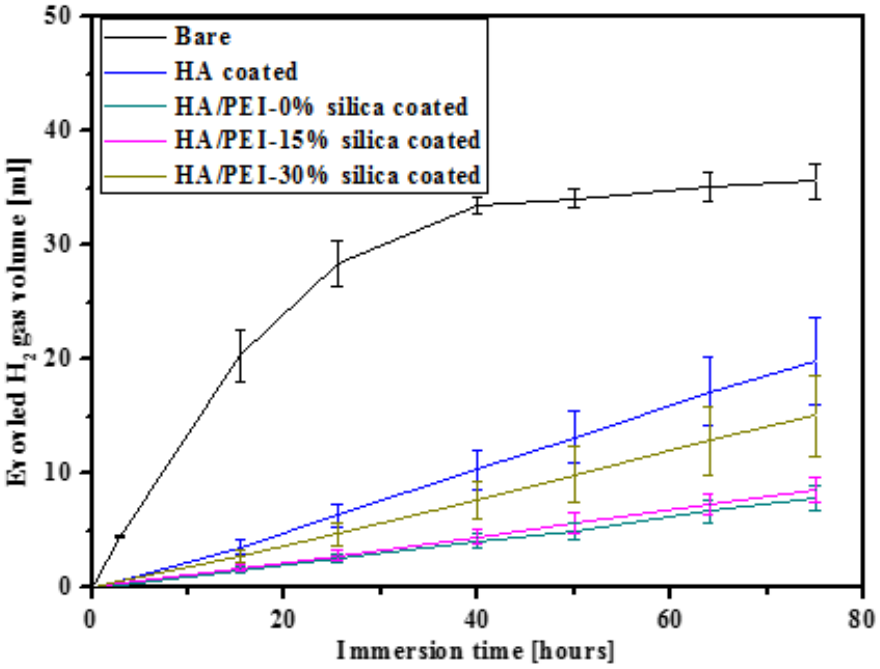

Figure 2.20. Volume of H_2 gas evolution after immersing bare, HA, and HA/PEI-Silica (0 vol%, 15 vol%, and 30 vol%) dual coated Mg in SBF

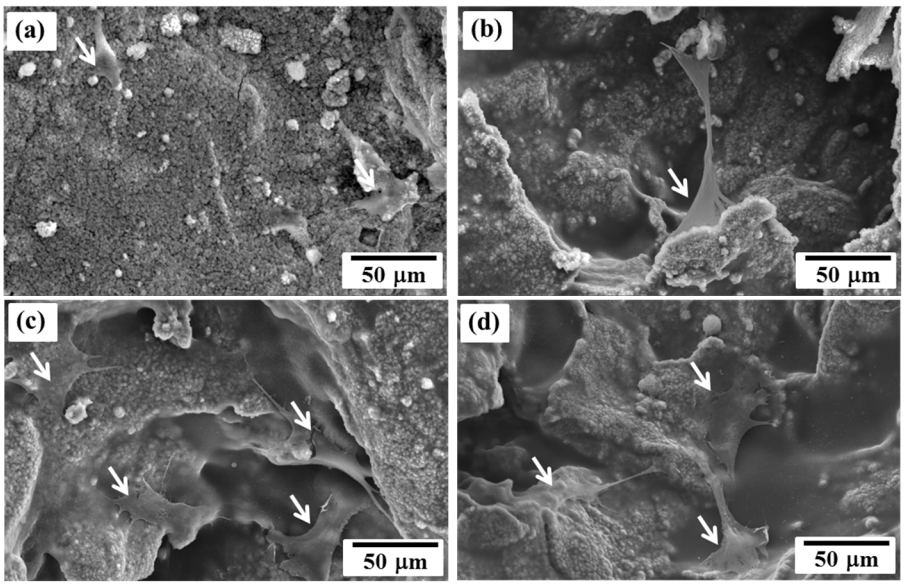

Figure 2.21. Initial MC3T3-E1 cell attachment on (a) HA, (b) HA/PEI-0% Silica, (c) HA/PEI-15% Silica, and (d) HA/PEI-30% Silica coated porous Mg after 6 hours culturing (arrows indicating cells)

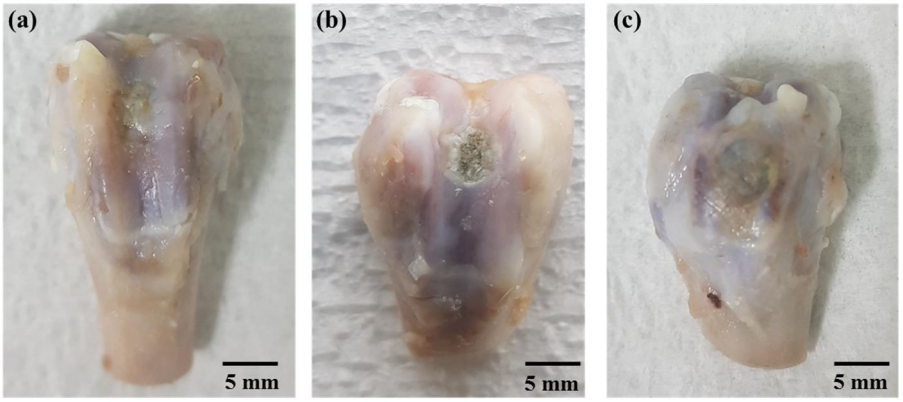

Figure 2.22. Representative rabbit femoropatellar images retrieved 5 weeks after implanting (a) HA coated, (b) HA/PEI coated and (c) HA/PEI-15% Silica coated biomimetic porous Mg

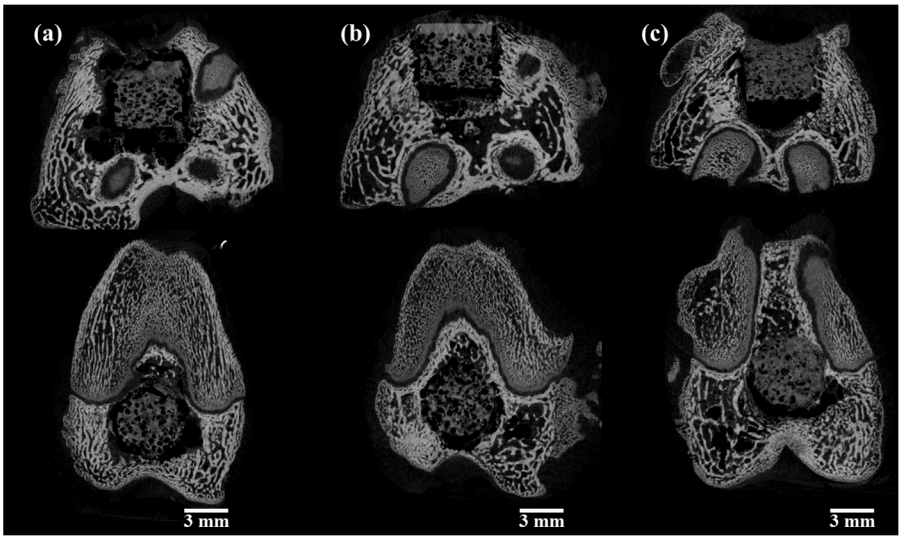

Figure 2.23. Cross-sectional μ-CT images of a representative rabbit femoropatellar bone after 5 weeks, (a) HA coated, (b) HA/PEI coated and (c) HA/PEI-15% Silica coated biomimetic porous Mg

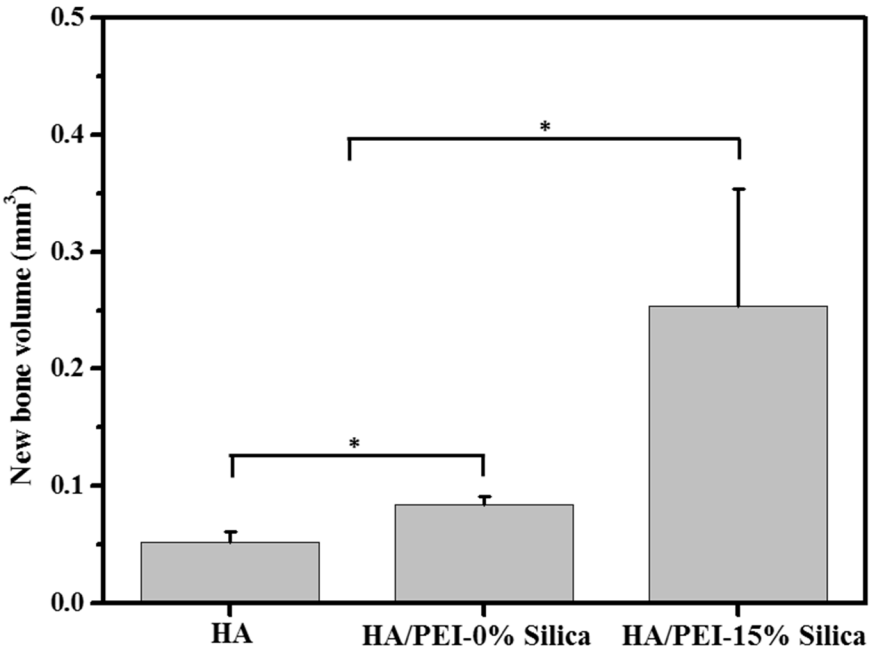

Figure 2.24. The new bone volume generated from HA coated, HA/PEI coated and HA/PEI-15% Silica coated biomimetic porous Mg at 5 weeks (*p < 0.05)

Chapter 3.

Selective PEI/PLGA Dual Coating on Mg for Biodegradable Drug Eluting Stent Applications

3.1. Introduction

Conventional bare metal stents (BMS) and drug eluting stents (DES) are mostly made of non-biodegradable materials. However, these non-biodegradable stents have problems such as stent migration due to the growth of blood vessels for pediatric patients, permanent physical irritation, limitation of re-stenting in identical site and late thrombosis [97-99]. Biodegradable stent could be the solution to these problems since it would be fully absorbed after the widening of the narrowed blood vessel and recovery of the damaged tissues [3, 97, 99].

Magnesium (Mg) and its alloys have been regarded as promising biodegradable stent materials. Mg has higher mechanical strength compared to other biodegradable polymers which enables to fabricate stents having high strength despite of the thin struts [100-103]. Furthermore, Mg is one of the essential elements used in human metabolism and it accelerates proliferation of endothelial cells [104-106]. However, rapid corrosion of Mg in physiological environments has limited the use of Mg in clinical applications. When rapid corrosion occurs, mechanical strength deteriorates severely, resulting in the stent collapse before the revascularization. Moreover, massive hydrogen gas generation and pH increase during the corrosion prohibit the endothelial cell attachment and proliferation, even worse, cause inflammatory

responses [107].

To protect Mg from rapid corrosion, various surface modifications such as micro arc-oxidation, anodization, fluoride or phosphate treatment, ion implantation and polymer coating were performed [1, 42, 46, 50, 54]. Among the various surface modifications, biodegradable polymer coating is beneficial for the stent application due to the corrosion protection and also its flexibility and stable drug release behavior. Because stents are expanded inside the blood vessel, coating material should be flexible to prevent delamination or crack formation during the expansion of the stent [100, 108]. Moreover, stents are often required to release anti-proliferative drugs such as paclitaxel or sirolimus to prohibit restenosis [100, 108-111]. Therefore, poly(lactic-co-glycolic acid) (PLGA) was coated on Mg as a corrosion protective drug carrier because of its considerable degradation rate and biocompatibility [112-115]. However, PLGA provided insufficient corrosion protection because of the low adhesion strength to Mg [116, 117]. Delamination of the polymer coating occurred during the corrosion results in the exposure of Mg which accelerates the corrosion. To prevent the delamination of the coating layer, polyetherimide (PEI) can be a great candidate for Mg stent coating material due to the good adhesion strength on Mg, additionally good biocompatibility with the endothelial cell [118]. However, because PEI is not suitable for the

drug release layer due to the high chemical stability, additional drug loaded polymer coating layer is necessary.

Therefore, PLGA loaded with anti-proliferative drug can be additionally coated on PEI coated Mg stent for the reliable drug release. Drug loaded in PLGA would restrain the rapid growth of smooth muscle cell [112, 114]. However, anti-proliferative drug could also prevent revascularization by prohibiting the attachment and proliferation of endothelial cell on the luminal area of the stent. Therefore, drug loaded PLGA layer should be only exposed to the abluminal area of the stent which is in contact with the blood vessel and only PEI layer should be exposed to the luminal area of the stent to accelerate the revascularization by restraining the rapid corrosion of Mg stent. Furthermore, due to the decrease of the corrosion rate PLGA layer would be stably attached to the Mg stent and the drug would be released stably. Figure 3.1. shows scheme of the selective PEI/PLGA dual coating on Mg stent and the main purpose of each coating layers.

In this study, gradually coated PEI and drug loaded PLGA dual layer is demonstrated as the coating material for Mg stent application. WE43 stent was selectively dual coated with PEI/PLGA and coating morphology was observed after expansion of the stent. To evaluate the corrosion protection of the coating layer dynamic corrosion test was performed on the condition

mimicking the blood flow and the structure and volume of the stent was evaluated with μ-CT. To evaluate release behavior of sirolimus and biological behavior of PEI/PLGA dual layer for the Mg stent coating, dual layer was spin-coated on Mg substrate. The release behavior of sirolimus which was loaded in dual coating layer was examined with UV spectrometer. Lastly, biological cell response on the coated specimens was examined by culturing human vascular endothelial cell (HUVEC) and vascular smooth muscle cell (VSMC) on the Mg specimens.

3.2. Experimental procedure

3.2.1. Sample preparation

WE43 Mg alloy (4.51 wt% yttrium, 2.05 wt% neodymium, 0.31 wt% zirconium, 0.051 wt% calcium, 0.011 wt% manganese, and balance Mg) specimens were prepared with the dimensions of 10 mm × 10 mm × 2 mm from commercial extruded WE43 Mg alloy supplied by commercial vendor (Yueyang Yuhua Yejin company, Beijing, China). The Mg specimens were polished with abrasive SiC papers from 400 to 1200 grit, and subsequently were cleansed with ethanol in an ultrasonic bath. PEI solution for coating material was prepared by dissolving PEI pellets (Sigma Aldrich, USA) in 1-Methyl- 2pyrrolidinone (NMP, Sigma Aldrich, USA) solvent by 15 w/v%. PLGA solution for coating material was prepared by dissolving PLGA pellets (lactide : glycolide = 65 : 35, M_w = 40,000-75,000, Sigma Aldrich, USA) in Tetrahydrofuran (THF, Sigma Aldrich, USA) solvent by 7.5 w/v%. PLGA was dissolved in THF to prevent the undesirable reaction and dissolution of PEI during dual coating PLGA on PEI coating layer. Pure PEI or PLGA were coated on Mg substrate by spin-coating at 3000 rpm for 1 min. The PEI coated specimen and PLGA coated specimen were dried at 70 °C and 37 °C respectively after spin coating for the dense PEI and PLGA coating layer with

perfect evaporation of the solvent. PEI/PLGA dual coating was performed by spin coating PEI on Mg substrate and spin coating PLGA on PEI coated Mg in sequence. PEI was fully dried in 70 °C oven for 1 day before PLGA dual coating and PLGA dual coated specimen was dried in 37 °C. For the drug loaded PLGA layer, sirolimus was dissolved in PLGA/THF solution by 3wt% and the solution was spin coated on PEI coated Mg specimen in the similar condition.

WE43 Mg alloy stent with a 15 mm length, 2 mm in diameter, and 150 μm strut thickness (Genoss, Korea) was prepared. PEI, PLGA or selective PEI/PLGA coating was performed by spray coater (Sonicoater, NOANIX, Korea). Mg stent was fixed at the end of the spray coater jig and PEI or PLGA was spray coated by the conditions shown in Table 3.1. Various parameters can be controlled during spray coating. Concentration of the polymer solution, distance from the stent and the spray nozzle, pressure of N_2 gas to spray the solution droplets, injection speed of the polymer solution, rotation speed of the stent and moving speed of the jig to the lateral way can be controlled. PEI and PLGA was spray coated 4 times each and coated stent was dried in 70 °C and 37 °C for 1 hr before every additional spray coating, respectively. Selective abluminal coating was performed by inserting the stent fully inside the jig. Figure 3.2. shows experimental procedure of selective PEI/PLGA dual

coating on Mg stent.

3.2.2. Characterization of selective PEI/PLGA coating

The surface morphology and thickness of the selective PEI/PLGA coating layers on Mg stent were observed by scanning electron microscopy (SEM, JSM-6360, JEOL, Japan) and focused ion beam (FIB, AURIGA, Carl Zeiss, Germany). Surface of the coated stent was observed after expansion in PBS (Welgene, Korea) at 37 °C. Scratch test was performed on PLGA or PEI/PLGA coated WE43 substrate with micro scratch tester (APEX-2T, Bruker, Germany). The velocity of the indenter was 2.5μm/s and the scratch distance was 500 μm.

3.2.3. *In-vitro* dynamic degradation test

Dynamic degradation tests were conducted by the experimental procedure designed to mimic the environment encountered by coronary stents with a constant laminar flow [119]. Simulated body fluid (SBF) was chosen as a circulating solution due to its stability and similar ion composition as human blood plasma [74]. PLGA or selective PEI/PLGA WE43 stent was expanded inside silicon rubber tubing (DAIHAN, Korea) with 3mm inner diameter in SBF solution at 37 °C after 1 min of stabilization. SBF solution was circulated

by the speed of 1 mL/min. At each predetermined period (0, 3, 7 and 14 days) 3D structure of the Mg stents were observed by μ-CT (Skyscan 1173, Kontich, Belgium). Furthermore, volume of the stent was measured using CTan software (Skyscan 1173, Kontich, Belgium).

3.2.4. Release behavior of sirolimus from PEI/PLGA coated Mg

Sirolimus loaded PLGA or PEI/PLGA dual coated Mg were immersed in PBS at 37 °C. The stability of drug loaded coating layer was observed by SEM. Specimens were taken out after 1 d immersion in PBS and rinsed with distilled water before SEM observation.

To quantify the amount of sirolimus loaded in coating layer, specimens were immersed in 5 mL of methylene chloride (MC, J.T.Baker, USA) and vortexed for 3 hours. After vortexing, the MC was fully evaporated in vacuum desiccator. 10 mL of methanol (J.T.Baker, USA) was added and vortexed for 1 min to dissolve sirolimus in methanol. Subsequently, 1ml of methanol was extracted with the syringe and absorbance values of sirolimus dissolved methanol was measured by UV spectroscopy at 278 nm, and then converted by a calibration curve. The calibration curve was prepared by measuring the optical absorbance values of sirolimus in 0.1-50 μg/mL methanol. The

obtained curve showed a linear relationship between the absorbance values and sirolimus concentration. Thus, each absorbance value was directly converted to the amount of sirolimus in each solution.

The release behavior of sirolimus was also monitored using UV spectroscopy by measuring the absorbance values of the released sirolimus at 278 nm. The sirolimus loaded PLGA or PEI/PLGA dual coated Mg were immersed in 3 mL of PBS with 0.05% of Tween20 (Sigma, USA) at 37 °C. The sirolimus released solutions were extracted at predetermined time and replaced with fresh PBS with 0.05% of Tween20. Prior to measuring optical absorbance values of the extracted solutions, the extracted solutions were mixed with 3 mL of MC and vortexed for 1 hour and MC was extracted with the syringe to the new vial and the MC was fully evaporated for 1 day. Subsequently, 3 mL of methanol was added and vortexed for 1 min to dissolve sirolimus remained in the vial. Absorbance values of sirolimus dissolved in methanol was measured by UV spectroscopy at 278 nm, and then converted by a calibration curve.

3.2.5. *In-vitro* biocompatibility test

To mimic the luminal surface of the stent, the initial cell adhesion and proliferation of human umbilical cord vein endothelial cells (HUVECs; ATCC,

CRL-1730) were performed. HUVECs were seeded on bare, PLGA or PEI coated Mg substrate as shown in Figure 3.10 (a). Furthermore, in-direct effect of sirolimus loaded on PLGA coating layer at abluminal surface to luminal surface of the stent was evaluated by the initial cell adhesion and proliferation of HUVEC. Cells were seeded on PEI coated Mg surface with PEI/PLGA dual coating on the bottom side of the specimen. Biological behaviors were compared depending on the existence of sirolimus in PLGA layer as shown in Figure 3.12 (a). To mimic the abluminal surface of the stent and evaluate the direct-effect of sirolimus, the initial cell adhesion and proliferation of vascular smooth muscle cell (VSMC, LONZA, CC-2583, Switzerland) were performed. VSMCs were seeded on PEI/PLGA dual coated Mg substrate and biological behaviors were evaluated depending on the existence of sirolimus in PLGA coating layer as shown in Figure 3.14 (a). Every specimen was cleansed in 70% ethanol and dried for 24h in a vacuum chamber. After drying the specimens, they were placed on a clean bench for 1 hour of sterilization with ultraviolet light. The cells were cultured in an alpha minimum essential medium (α-MEM, Welgene, USA) supplemented with 5% fetal bovine serum (FBS, Gibco, USA) and 1% penicillin-streptomycin (Pen strep, Gibco, USA) in a humid incubator with 5% CO_2 at 37 °C. The initial cell attachment was observed with confocal laser scanning microscope (CLSM, Fluoview FV1000,

Olympus, Japan) after 1 day of cell seeding with the density of 5×10^4 cells/mL. Prior to the CLSM observation, the cells were fixed with 4% paraformaldehyde solution diluted with PBS for 10 min, and washed with PBS 2 times. After that, cells were permeabilized with 0.1% Triton X-100 (Sigma-Aldrich, USA) diluted with PBS for 5 min, and then washed with PBS 2 times. Blocking the nonspecific site was performed with 1% bovine serum albumin (BSA, Sigma-Aldrich, USA), followed by staining of F-actin and nuclei of the cells with phalloidin (Alexa Fluor® 555 phalloidin, Molecular Probes, USA) and 4',5-diamidino-2-phenylindole (DAPI, ProLong Gold® antifade reagent with DAPI, Invitrogen, USA), respectively. Cell proliferation was determined after 1 and 3 days of culturing for evaluating the biocompatibility of coating layers on Mg with HUVEC and 3 and 5 days of culturing for evaluating in-direct and direct effect of sirolimus with HUVEC and VSMC respectively. Cell seeding density was 3×10^4 cells/mL. DNA analysis was performed using Cyquant® cell proliferation assay kit (C7026, Invitrogen, USA). Before measurements, the cells that adhered to the specimens were detached and suspended in a fluorescent dye solution. The DNA amount of the detached cells was measured using a multiple plate reader (Victor3, PerkinElmer, USA) at 480/535 nm wavelength. The measured

florescence values were converted to the DNA amount using a DNA standard curve. The standard curve was prepared by measuring the florescence values of DNA in buffer solution. In this assay kit, the DNA level was directly proportional to the number of living cells.

3.2.6. Statistical analysis

All data are expressed as mean ± standard deviation (SD). The statistical analysis was performed by one-way analysis of variance with Bonferroni's post-hoc comparison. A p value inferior to 0.05 was considered statistically significant in all cases.

3.3. Results and discussion

3.3.1. Characterization of selective PEI/PLGA dual coated Mg stent

The selective PEI/PLGA dual coated Mg stent was designed to expose two different surfaces, luminal surface with PEI coating layer and abluminal surface with PEI/PLGA coating layer which PLGA is exposed as shown in Figure 3.1. It was achieved by sequential spray coating with PEI full coating and PLGA asymmetric coating (Figure 3.2.). The surface morphologies of bare WE43 stent and selective PEI/PLGA dual coated stent was observed. The neodymium (Nd) and yttrium (Y) second phase precipitates were found on the surface of bare WE43 stent (Figure 3.3. (a)) which were formed during the electro-polishing of the stent [31]. After the selective PEI/PLGA dual coating these second phase precipitates were covered by the polymer layer. Moreover, after the expansion of the stent defects or delamination was not found indicating that the coating layers were stably adhered on Mg stent (Figure 3.3. (b)). The thickness of the selective PEI/PLGA dual coated stent were observed on each luminal and abluminal surfaces of the stent as shown in Figure. 3.3. (c) and (d). It was observed that the thickness of PEI on the luminal side of the stent was ~ 300 nm. On the

contrary, on the abluminal side two layers were observed with ~ 300 nm thickness each, indicating the PEI/PLGA dual layer. Selective dual coating with spray coating method successfully made distinctively asymmetrical coating layers on luminal and abluminal side of the stent. Therefore, the selective dual coating method could be reproduced on actual stent, leading to production of the dual-functionalized stent with two different polymer surfaces.

Figure 3.4. shows SEM images of scratch profiles generated from progressive load scratch testing on an PLGA or PEI/PLGA dual coated Mg substrate. It appears that the scratch profile in PLGA coating is similar to that of the PEI/PLGA dual coating at lower scratch loads. This is because the surface polymer is both PLGA for mono and dual coating layer. However, as the scratch load increases cracks started to appear earlier from the PLGA coated Mg. Moreover, delamination of the coating layer started earlier at the PLGA coated specimen than dual coated specimen. It indicates that PEI inter layer has higher adhesion strength with Mg than that of PLGA and eventually results in better corrosion protection of Mg provided by PEI/PLGA dual coating than PLGA coating [120]. Furthermore, on the delamination site Mg substrate appears rather than smooth polymer layer such as PLGA layer. It indicates that PLGA has good interaction with the PEI interlayer.

3.3.2. Corrosion behavior of selective PEI/PLGA coated Mg stent

Uncoated Mg stent and PLGA or selective PEI/PLGA coated Mg stents were immersed in circulating SBF solution. Morphology of the stents were observed and the residual volume of the stents were evaluated with μ-CT. Uncoated Mg stent started to corroded rapidly losing the innate metal color compared with coated stents from 1 day as shown in Figure 3.5. Furthermore, after 3 days struts of the bare stent started to wash out by the flow of SBF and PLGA coated stent also started to corrode rapidly. However, selective PEI/PLGA dual coated stent remained the shape until 3 days, showing the good corrosion resistance. The dynamic degradation rate of the selective PEI/PLGA coated Mg stent was significantly lower than that of the uncoated and PLGA coated Mg stent (Figure 3.6. and Figure 3.7.). The uncoated Mg stent corroded rapidly and the struts of the stent were removed by the flow of SBF as shown in Figure 3.6. PLGA coated Mg stent seemed to maintain its shape until 3 day of the corrosion test. However, corrosion started to occur rapidly from 7 days. In contrary, selective PEI/PLGA coated Mg stent maintained its shape until 7 days and from 14 days struts on the end of the

stent were partially removed due to the local corrosion. Residual volume of the stent calculated by μ-CT also shows that degradation rate of the selective PEI/PLGA coated Mg stent was significantly lower than that of the uncoated and PLGA coated Mg stent as shown in Figure 3.7. PLGA coating improved the corrosion resistance in the early state, however, due to the low adhesion strength and stability of PLGA coating corrosion was accelerated after some period of time [116, 117]. In contrary, selective PEI/PLGA dual coated stent has good corrosion resistance due to the full coated PEI which has good adhesion strength and stability results in good corrosion resistant of the coating layer [46, 88].

3.3.3. Drug release behavior of PEI/PLGA coated Mg stent

The effects of the PEI interlayer on sirolimus loaded PLGA were shown in Figure 3.8. and Figure 3.9. After immersing sirolimus loaded PLGA or PEI/PLGA dual coated Mg substrate in PBS for 1 day, surface morphology was observed by SEM (Figure 3.8.). Delamination occurred severely on PLGA coated specimen, whereas, PEI/PLGA dual coated specimen showed stable morphology of PLGA coating layer. PEI interlayer had a great role of

improving corrosion resistance [46, 88] and prohibiting the delamination of PLGA from PEI interlayer. Furthermore, the cumulative sirolimus release profiles were shown in Figure 3.9. The total average amount of loaded sirolimus was ~ 0.5 μg/mm^2. PLGA coated Mg showed a burst release of sirolimus compared with PEI/PLGA dual coated Mg. After 14 days, PLGA coated specimen released 79% of the total amount of sirolimus. On the contrary, the amount of sirolimus released from the PEI/PLGA dual coated specimen was 62% of the total amount of sirolimus. After 17 days both PLGA and PEI/PLGA coated specimens released almost 90% of sirolimus and after 21 days the release amount saturated. According to these results, it is suggested that the introduction of PEI coating at the interface between stent surface and PLGA layer could promote an efficient sirolimus release from PLGA matrix.

3.3.4. *In-vitro* biocompatibility test

The cell viability and proliferation tests were conducted using HUVECs and VSMCs. Firstly, to mimic the luminal surface of the stent, HUVECs were seeded on bare, PLGA or PEI coated Mg substrate as shown in Figure 3.10 (a). Figure 3.10. (b) shows the initial cell adhesion on bare, PLGA or PEI coated Mg substrate. On the bare Mg, cells were hardly observed, in a

round shape with minimal spreading. The poor cell attachment on bare Mg has been attributed to the rapid pH increase and H_2 evolution during corrosion [29, 50, 93]. However, the large amount of cells was strongly attached on PLGA and PEI coated Mg, with well spread out and flattened shape of HUVECs. It is also can be observed by the DNA analysis result as shown in Figure 3.11. At 1 day the DNA amount which is proportional to the cell amount is higher on both coated Mg. However, after 3 days cell amount decreased on PLGA coated specimen, whereas, PEI coated specimen had highest DNA amount and even increased than 1 day. This is due to the un-stability of PLGA coating layer on Mg resulting in the rapid corrosion of Mg. PEI coating layer improved the corrosion resistance and showing good biocompatibility with HUVEC [46, 88, 118].

Furthermore, to evaluate the in-direct effect of sirolimus loaded in PLGA coating layer from abluminal surface to luminal surface of the stent, HUVECs were seeded on PEI coated Mg surface with PEI/PLGA dual coating on the bottom side of the specimen. Biological behaviors were compared depending on the existence of sirolimus in PLGA layer as shown in Figure 3.12 (a). Figure 3.12. (b) shows the initial cell adhesion on PEI coating layer depending on the existence of sirolimus in PLGA coating layer which is beneath the Mg substrate. Both specimens had large amount of cells adhered

on PEI coating layer with well spread out and flattened shape. To check the effect for longer period of time, proliferation was also evaluated for 3 and 5 days. As shown in Figure 3.13., DNA analysis showed high cell viability for both specimens despite of the existence of sirolimus at 3 and 5 days. It indicates that by the selective PEI/PLGA dual coating on Mg stent, amount of released sirolimus from abluminal side will have almost no adverse effect on HUVEC adhesion and proliferation on PEI coating layer at luminal side of the stent.

To mimic the abluminal surface of the stent and evaluate the direct effect of sirolimus, VSMCs were seeded on PEI/PLGA dual coated Mg substrate and biological behaviors were evaluated depending on the existence of sirolimus in PLGA coating layer as shown in Figure 3.14 (a). Figure 3.14. (b) shows the initial cell adhesion of VSMC after 1day. High viability of well spread VSMC was seen on PEI/PLGA dual coated Mg without sirolimus, due to good biocompatibility of PLGA and good corrosion resistance of PEI/PLGA dual coating. On the contrary, on PEI/PLGA dual coated specimen with sirolimus had low viability of cells with an almost round shape with minimal spreading. Figure 3.15. shows the proliferation of VSMC. PEI/PLGA coated specimen without sirolimus in PLGA layer had high viability of cells and with good proliferation, whereas, PEI/PLGA coated specimen with

sirolimus had low amount of cells at both 3 and 5 days. The poor cell attachment and proliferation of VSMC on PEI/PLGA dual coated Mg has been mainly attributed to the effect of sirolimus [112, 114].

3.4. Conclusions

We have demonstrated a drug loaded selective PEI/PLGA dual coating by full PEI coating and subsequent abluminal PLGA coating loaded with sirolimus on Mg stent for biodegradable drug eluting Mg stent. The PEI which has good adhesion strength and good biocompatibility improved both corrosion resistance and biocompatibility with HUVEC. Excellent corrosion resistance of PEI worked as good interlayer between Mg substrate and sirolimus loaded PLGA coating layer to prohibit the delamination of PLGA coating layer by preventing the rapid corrosion of Mg stent. Furthermore, good biocompatibility of PEI with HUVEC worked as good coating layer on luminal side of the stent showing excellent cell adhesion and proliferation of HUVEC. PLGA was a good drug eluting polymer coating layer and loaded sirolimus effectively suppressed cell adhesion and proliferation of VSMC and almost no adverse effect on HUVEC at the luminal side of the stent. Consequently, sirolimus loaded selective PEI/PLGA dual coating on Mg stent offers a promising approach for the development of biodegradable drug eluting cardiovascular stents.

Polymer	Solvent	Ratio (w/v%)	Distance (mm)	N_2 pressure (kgf/cm^2)	Injection speed (μl/min)	Rotation speed (rpm)	Moving velocity (m/s)
PEI	**NMP**	**3**	**90**	**2**	**100**	**30**	**1**
PLGA	**THF**	**1.5**	**20**	**2**	**300**	**100**	**5**

Table 3.1. Parameters of spray coating PEI and PLGA on Mg stent

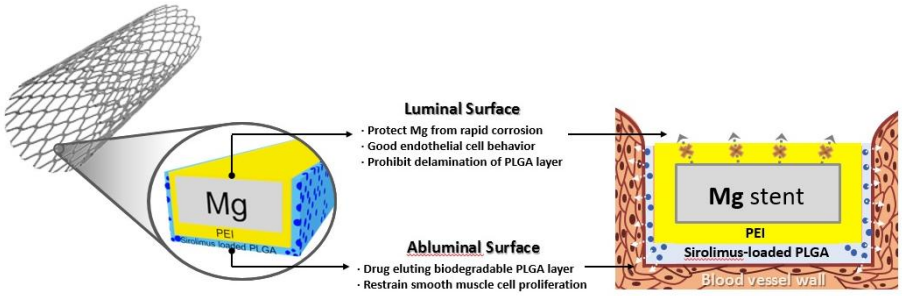

Figure 3.1. Scheme of selective PEI/PLGA dual coated Mg stent and the purpose of PEI and PLGA coating layer corresponding to luminal and abluminal surface, respectively

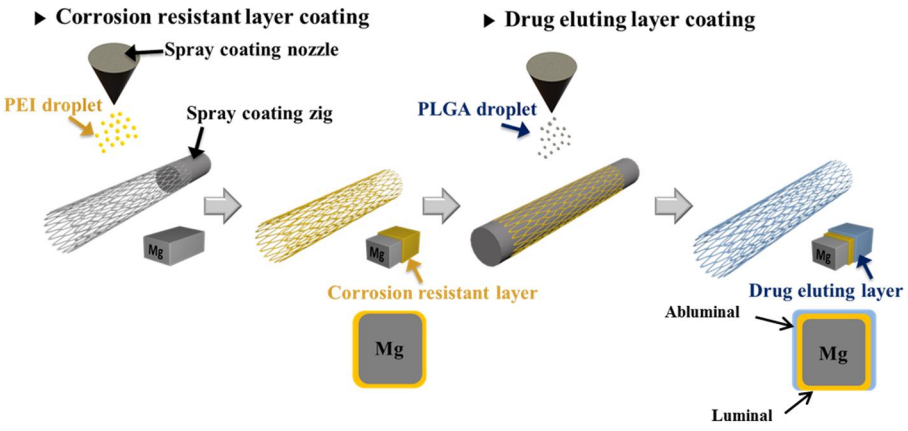

Figure 3.2. Selective PEI/PLGA dual coating by spray coating process

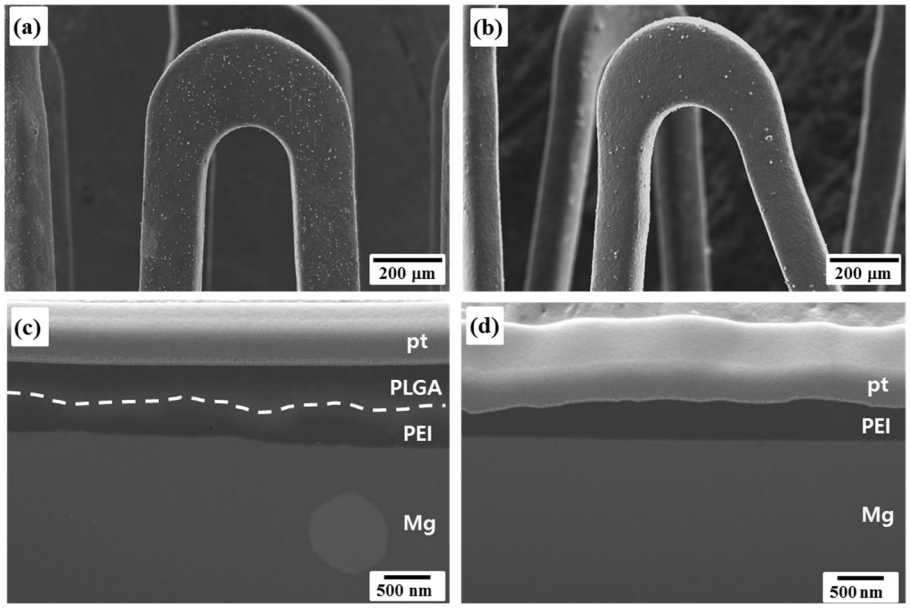

Figure 3.3. Surface morphology of (a) uncoated and (b) selective PEI/PLGA dual coated Mg stent, and cross sectional image of selective dual coated Mg stent on (c) abluminal and (d) luminal side of the stent

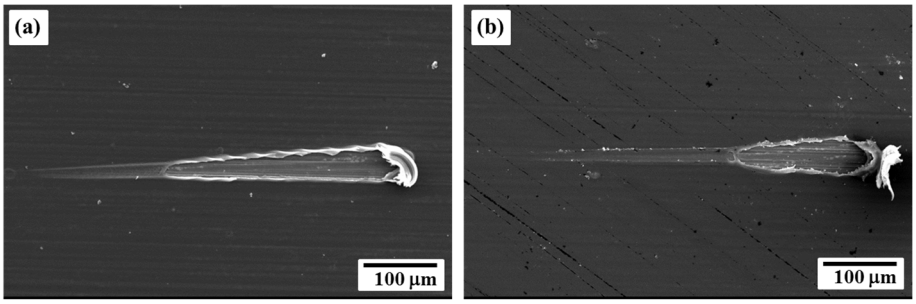

Figure 3.4. Coating morphology of (a) PLGA coated and (b) PEI/PLGA dual coated Mg after scratch test

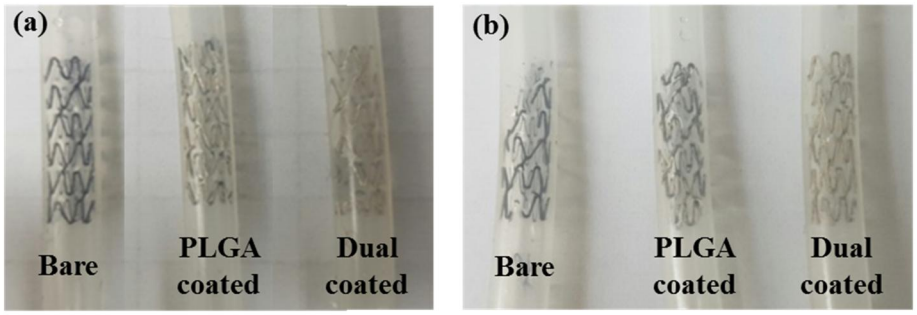

Figure 3.5. Optic images of uncoated, PLGA coated or selective PEI/PLGA dual coated Mg stent in silicon tube with circulation of SBF solution after (a) 1 day and (b) 3 days

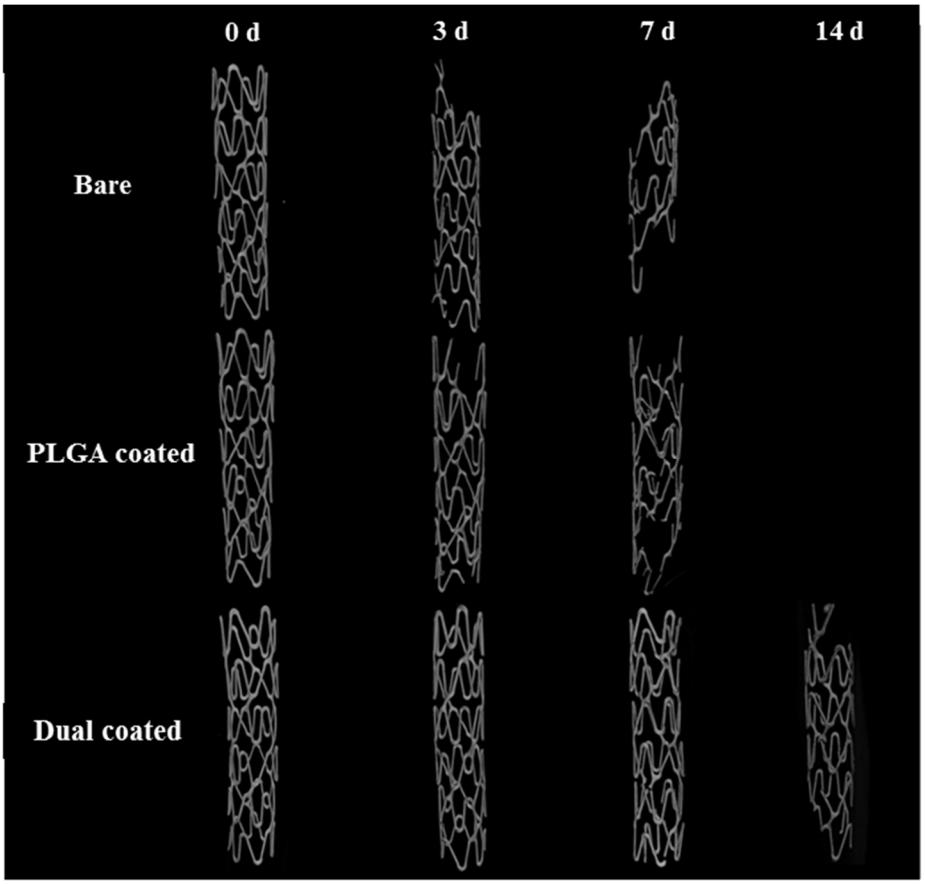

Figure 3.6. 3D structural μ-CT image of uncoated, PLGA coated, and selective PEI/PLGA dual coated Mg stent during dynamic corrosion test

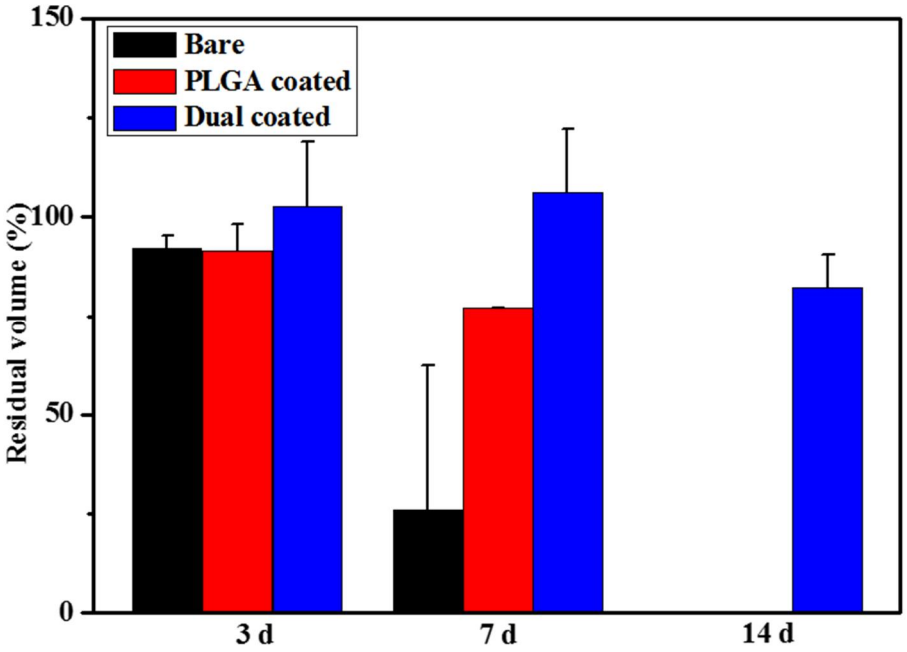

Figure 3.7. Residual volume of uncoated, PLGA coated, and selective dual coated Mg stent during dynamic corrosion test

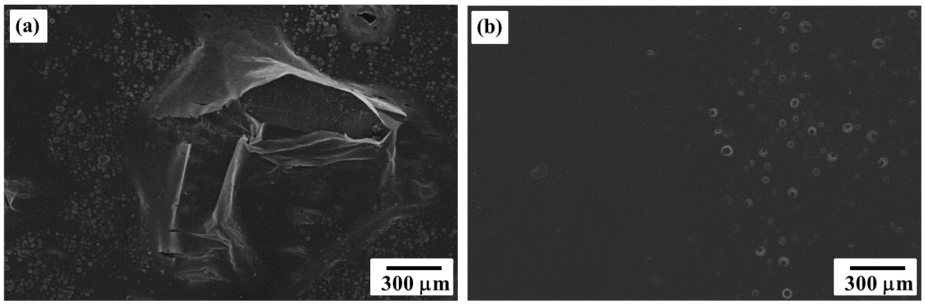

Figure 3.8. Surface morphology of sirolimus loaded (a) PLGA and (b) PEI/PLGA dual coating layer on Mg after 1 day immersion in PBS

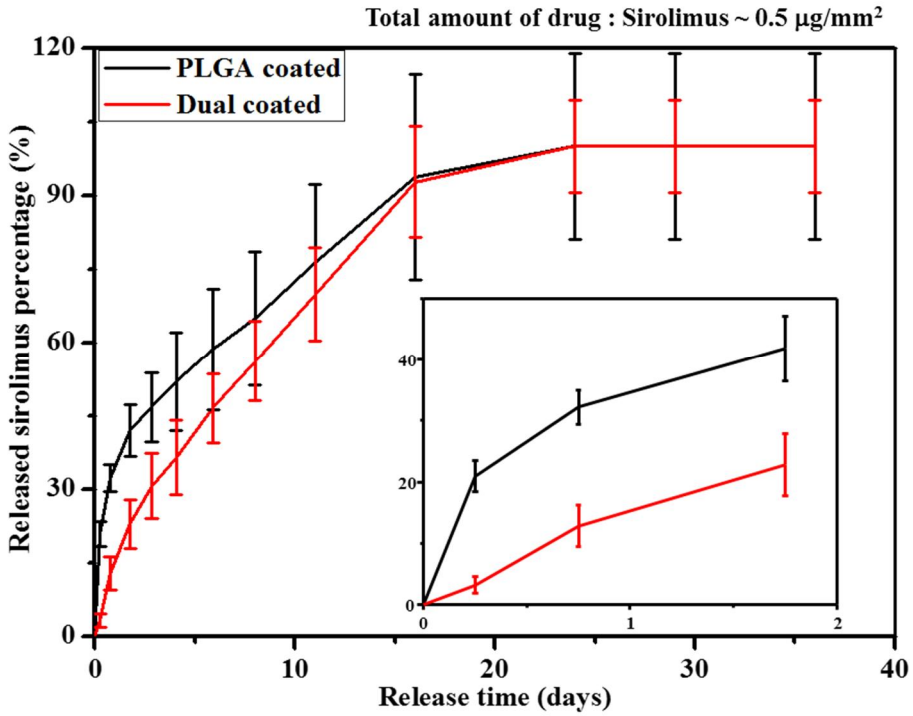

Figure 3.9. Sirolimus release profile of drug loaded PLGA and PEI/PLGA dual coated Mg in PBS

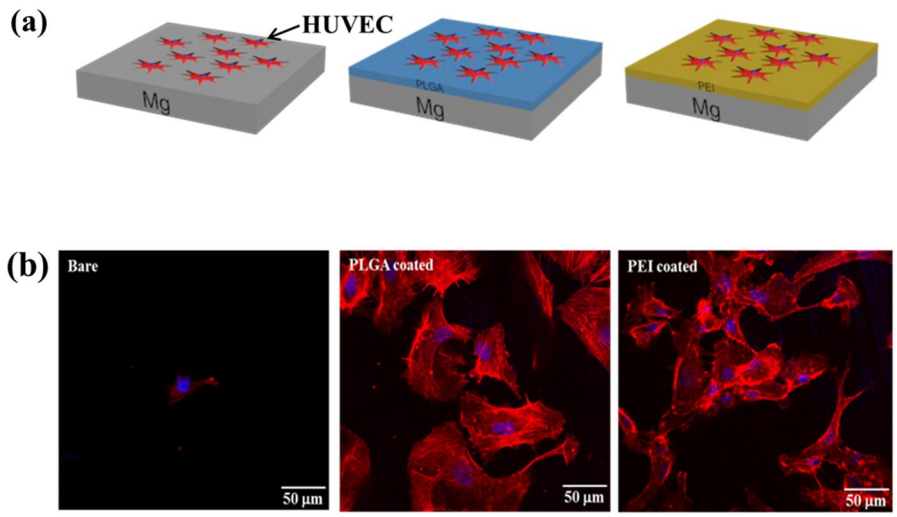

Figure 3.10. (a) Scheme of the *in-vitro* cell test procedure and (b) initial cell attachment of HUVEC on uncoated, PLGA or PEI coated Mg after 1 day culturing

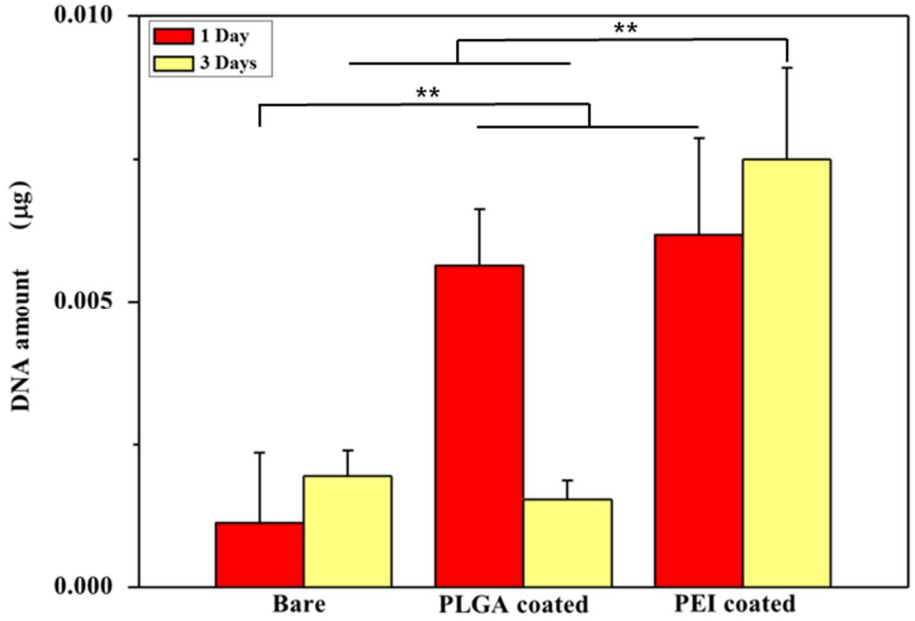

Figure 3.11. Proliferation of HUVEC on uncoated, PLGA or PEI coated Mg (**$p < 0.005$)

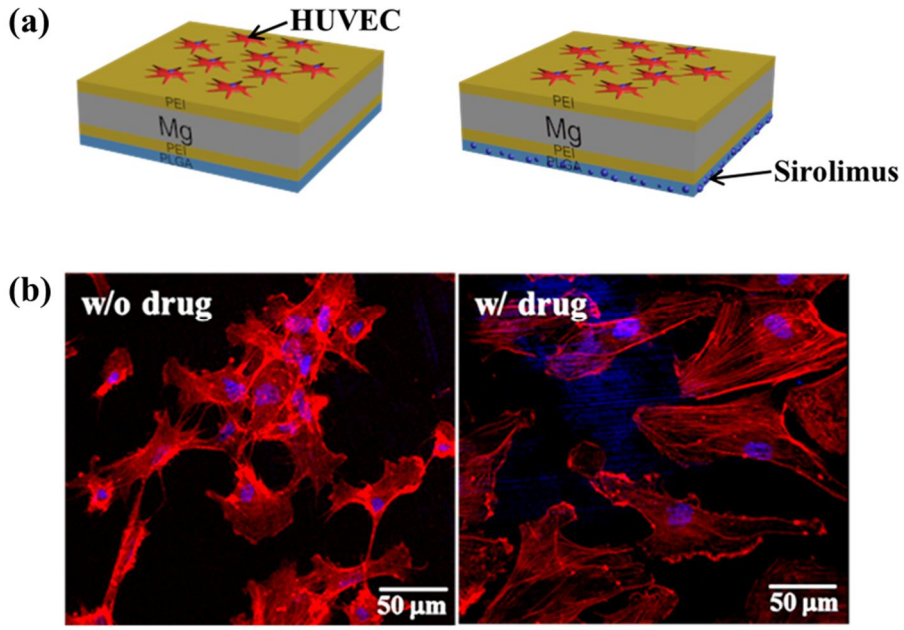

Figure 3.12. In-direct effect of sirolimus on HUVEC at luminal side of the stent; (a) Scheme of the *in-vitro* cell test procedure and (b) initial cell attachment on PEI coated Mg depending on the existence of sirolimus in PLGA coating layer at abluminal side of the stent

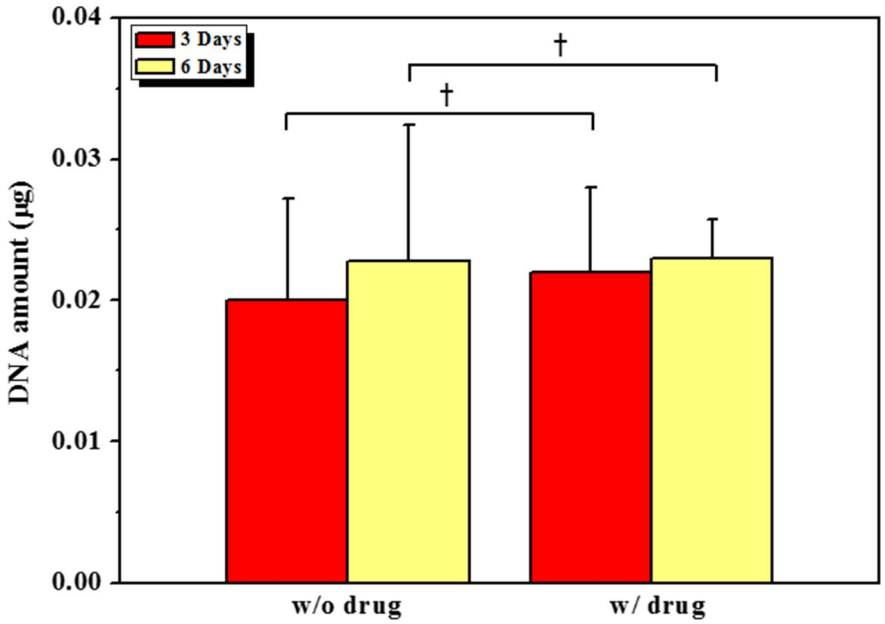

Figure 3.13. In-direct effect of sirolimus on HUVEC at luminal side of the stent; Proliferation on PEI coated Mg depending on the existence of sirolimus in PLGA coating layer at abluminal side of the stent (†$p > 0.05$)

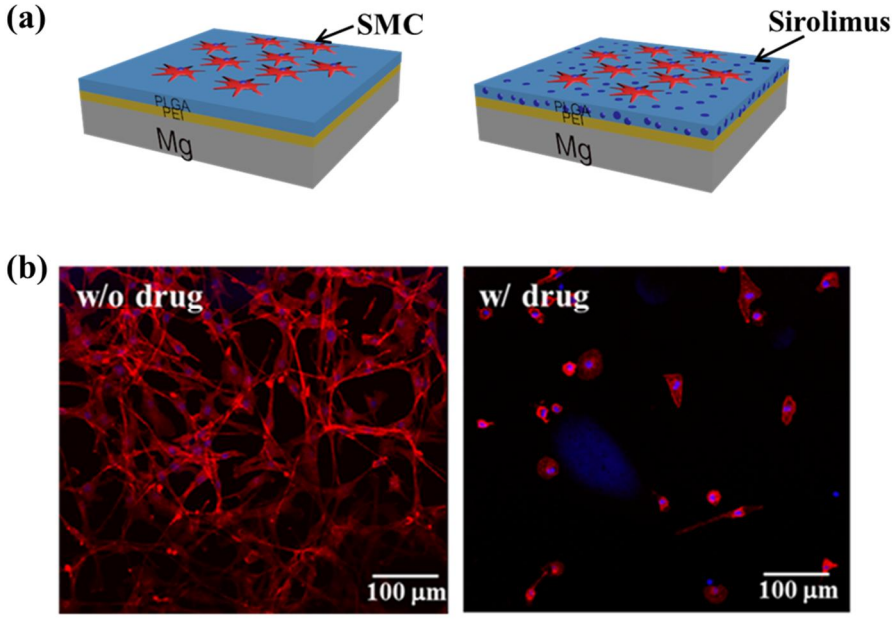

Figure 3.14. Direct effect of sirolimus on SMC at abluminal side of the stent; (a) Scheme of the in-vitro cell test procedure and (b) initial cell attachment on PEI/PLGA dual coated Mg depending on the existence of sirolimus in PLGA coating layer

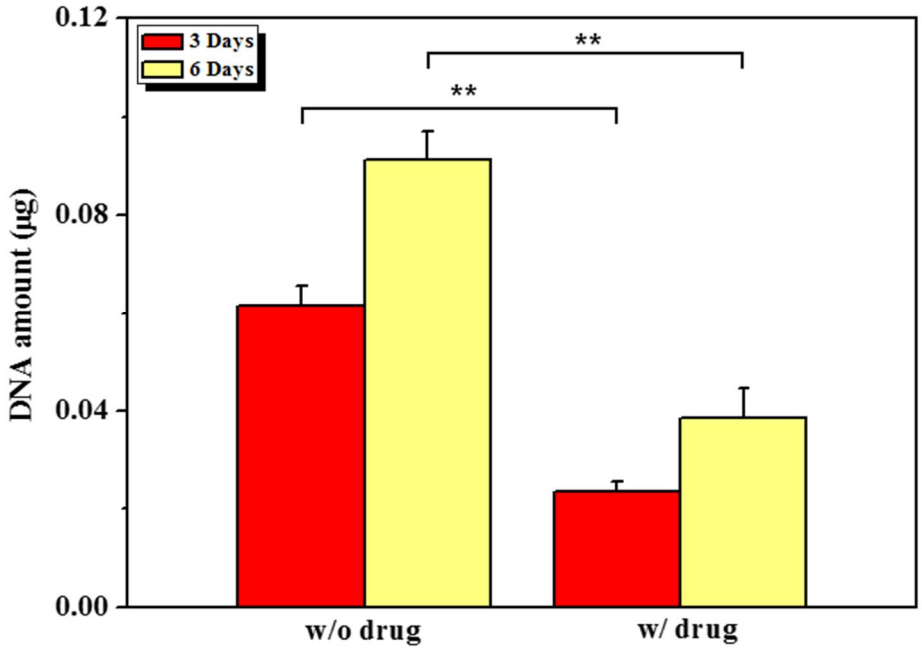

Figure 3.15. Direct effect of sirolimus on SMC at abluminal side of the stent; Proliferation on PEI/PLGA dual coated Mg depending on the existence of sirolimus in PLGA coating layer (**$p < 0.005$)

Chapter 4.

Conclusions

4.1. Conclusions

In this thesis, we aimed to develop a Mg implant that fulfills the two main requirements necessary for the biodegradable medical applications, namely a low corrosion rate and a good biocompatibility. Furthermore, improving the function of these biodegradable implants by fulfilling these main requirements, especially for dental/orthopedic and vascular stent applications.

Firstly, from chapter 2 for dental and orthopedic application biomimetic porous Mg with dense/porous combined structure was fabricated by SPS and space holder process for high strength and pore interconnectivity. Biomimetic porous Mg had significantly higher mechanical properties compared with porous Mg while maintaining the high interconnectivity of the pores. Furthermore, to decrease the corrosion rate HA was coated on the porous Mg by aqueous precipitation method. However, due to the brittle performance of HA, cracks formed on the coating layer propagating to the Mg substrate. Cracks effected critically on rapid corrosion due to the complex shape and large surface area of porous Mg. Consequently, additional polymer layer was needed to be dual coated on the HA layer to cover the cracks and improve the corrosion resistance. PEI was a good candidate for the polymer dual coating layer due to the high stability. However, due to the deficiency of

bioactivity of PEI, bioactive silica nano-particle was hybridized by sol-gel method. By sol-gel method silica nano-particles were dispersed well in the PEI matrix compared with simple mixing of the silica nano-particle. This PEI-Silica hybrid coating on HA layer inhibited the corrosion of porous Mg remarkably in the SBF solution. Furthermore, the *in-vitro* cell test and *in-vivo* animal test showed the significant improvement of biological activity of PEI-Silica hybrid coated biomimetic Mg scaffold.

Lastly, chapter 3 focused on the vascular stent application by selective PEI/PLGA dual coating for biodegradable drug eluting stent. Selective PEI/PLGA coating was performed by spray coating process. PEI was fully coated on Mg stent for good corrosion resistance and biocompatibility with HUVEC. Subsequently, anti-proliferative drug loaded PLGA was coated on the abluminal side of the stent for selective drug release to the blood vessel wall to prohibit the excessive proliferation of smooth muscle cell and restenosis. Selective PEI/PLGA coating was successfully performed by spray coating and this coating decreased the corrosion rate of Mg stent in the dynamic corrosion test mimicking the real blood flow. Due to the improvement of corrosion resistance of Mg stent, sirolimus was released stably and both cell attachment and proliferation of HUVEC were improved remarkably. Furthermore, released sirolimus effectively suppressed the VSMC

attachment and proliferation indicating for the prevention of restenosis.

This study suggest that PEI-Silica coated biomimetic Mg and selective PEI/PLGA dual coated Mg stent offered a great potential for dental/orthopedic and vascular stent applications. Depending on these applications, HA/PEI-Silica and selective PEI/PLGA dual coating can improve the functions of the implants by enhancing the corrosion resistance and biocompatibility. Therefore, the study highlighted the functional coatings to actively apply Mg to biodegradable medical applications.

Reference

[1] M.P. Staiger, A.M. Pietak, J. Huadmai, G. Dias, Magnesium and its alloys as orthopedic biomaterials: A review, Biomaterials 27(9) (2006) 1728-1734.
[2] O. Bostman, H. Pihlajamaki, Clinical biocompatibility of biodegradable orthopaedic implants for internal fixation: a review, Biomaterials 21(24) (2000) 2615-2621.
[3] N. Grabow, D.P. Martin, K.P. Schmitz, K. Sternberg, Absorbable polymer stent technologies for vascular regeneration, J Chem Technol Biot 85(6) (2010) 744-751.
[4] G.L. Song, Control of biodegradation of biocompatable magnesium alloys, Corros Sci 49(4) (2007) 1696-1701.
[5] C. Seal, K. Vince, M. Hodgson, Biodegradable surgical implants based on magnesium alloys–A review of current research, IOP conference series: materials science and engineering, IOP Publishing, 2009, p. 012011.
[6] J.E. Gray, B. Luan, Protective coatings on magnesium and its alloys - a critical review, J Alloy Compd 336(1-2) (2002) 88-113.
[7] G.L. Song, A. Atrens, Corrosion mechanisms of magnesium alloys, Adv Eng Mater 1(1) (1999) 11-33.
[8] R.C. Zeng, W. Dietzel, F. Witte, N. Hort, C. Blawert, Progress and challenge for magnesium alloys as biomaterials, Adv Eng Mater 10(8) (2008) B3-B14.
[9] N.E.L. Saris, E. Mervaala, H. Karppanen, J.A. Khawaja, A. Lewenstam, Magnesium - An update on physiological, clinical and analytical aspects, Clin Chim Acta 294(1-2) (2000) 1-26.
[10] C. Castellani, R.A. Lindtner, P. Hausbrandt, E. Tschegg, S.E. Stanzl-Tschegg, G. Zanoni, S. Beck, A.M. Weinberg, Bone-implant interface strength and osseointegration: Biodegradable magnesium alloy versus standard titanium control, Acta Biomater 7(1) (2011) 432-440.
[11] Z.J. Li, X.N. Gu, S.Q. Lou, Y.F. Zheng, The development of binary Mg-Ca alloys for use as biodegradable materials within bone, Biomaterials 29(10) (2008) 1329-1344.
[12] G.L. Song, A. Atrens, Understanding magnesium corrosion - A framework for improved alloy performance, Adv Eng Mater 5(12) (2003) 837-858.
[13] G.W. Murphy, Pourbaix,M - Atlas of Electrochemical Equilibria in Aqueous Solutions, Science 154(3756) (1966) 1537-&.
[14] Y.C. Xin, K.F. Huo, H. Tao, G.Y. Tang, P.K. Chu, Influence of aggressive

ions on the degradation behavior of biomedical magnesium alloy in physiological environment, Acta Biomater 4(6) (2008) 2008-2015.
[15] G.E.J. Poinern, S. Brundavanam, D. Fawcett, Biomedical magnesium alloys: a review of material properties, surface modifications and potential as a biodegradable orthopaedic implant, American Journal of Biomedical Engineering 2(6) (2012) 218-240.
[16] J.X. Yang, F.Z. Cui, Q.S. Yin, Y. Zhang, T. Zhang, X.M. Wang, Characterization and Degradation Study of Calcium Phosphate Coating on Magnesium Alloy Bone Implant In Vitro, Ieee T Plasma Sci 37(7) (2009) 1161-1168.
[17] Y.F. Zheng, X.N. Gu, F. Witte, Biodegradable metals, Mat Sci Eng R 77 (2014) 1-34.
[18] S. Shadanbaz, G.J. Dias, Calcium phosphate coatings on magnesium alloys for biomedical applications: A review, Acta Biomater 8(1) (2012) 20-30.
[19] F. Geng, L.L. Tan, X.X. Jin, J.Y. Yang, K. Yang, The preparation, cytocompatibility, and in vitro biodegradation study of pure beta-TCP on magnesium, J Mater Sci-Mater M 20(5) (2009) 1149-1157.
[20] J.E. Gray-Munro, C. Seguin, M. Strong, Influence of surface modification on the in vitro corrosion rate of magnesium alloy AZ31, J Biomed Mater Res A 91a(1) (2009) 221-230.
[21] L.P. Xu, F. Pan, G.N. Yu, L. Yang, E.L. Zhang, K. Yang, In vitro and in vivo evaluation of the surface bioactivity of a calcium phosphate coated magnesium alloy, Biomaterials 30(8) (2009) 1512-1523.
[22] Y.J. Zhang, G.Z. Zhang, M. Wei, Controlling the Biodegradation Rate of Magnesium Using Biomimetic Apatite Coating, J Biomed Mater Res B 89b(2) (2009) 408-414.
[23] S.V. Dorozhkin, Calcium orthophosphate coatings on magnesium and its biodegradable alloys, Acta Biomater 10(7) (2014) 2919-2934.
[24] P.B. Srinivasan, J. Liang, C. Blawert, M. Stormer, W. Dietzel, Characterization of calcium containing plasma electrolytic oxidation coatings on AM50 magnesium alloy, Appl Surf Sci 256(12) (2010) 4017-4022.
[25] M. Razavi, M. Fathi, O. Savabi, D. Vashaee, L. Tayebi, In vivo assessments of bioabsorbable AZ91 magnesium implants coated with nanostructured fluoridated hydroxyapatite by MAO/EPD technique for biomedical applications, Mat Sci Eng C-Mater 48 (2015) 21-27.
[26] H.X. Wang, S.K. Guan, X. Wang, C.X. Ren, L.G. Wang, In vitro degradation and mechanical integrity of Mg-Zn-Ca alloy coated with Ca-deficient hydroxyapatite by the pulse electrodeposition process, Acta Biomater 6(5) (2010) 1743-1748.
[27] H.X. Wang, S.K. Guan, Y.S. Wang, H.J. Liu, H.T. Wang, L.G. Wang, C.X.

Ren, S.J. Zhu, K.S. Chen, In vivo degradation behavior of Ca-deficient hydroxyapatite coated Mg-Zn-Ca alloy for bone implant application, Colloid Surface B 88(1) (2011) 254-259.
[28] C.-C. Chen, J.-Y. Chueh, H. Tseng, H.-M. Huang, S.-Y. Lee, Preparation and characterization of biodegradable PLA polymeric blends, Biomaterials 24(7) (2003) 1167-1173.
[29] L.P. Xu, A. Yamamoto, Characteristics and cytocompatibility of biodegradable polymer film on magnesium by spin coating, Colloid Surface B 93 (2012) 67-74.
[30] L.P. Xu, A. Yamamoto, In vitro degradation of biodegradable polymer-coated magnesium under cell culture condition, Appl Surf Sci 258(17) (2012) 6353-6358.
[31] M. Diez, M.H. Kang, S.M. Kim, H.E. Kim, J. Song, Hydroxyapatite (HA)/poly-L-lactic acid (PLLA) dual coating on magnesium alloy under deformation for biomedical applications, Journal of materials science. Materials in medicine 27(2) (2016) 34.
[32] X.N. Gu, Y.F. Zheng, Q.X. Lan, Y. Cheng, Z.X. Zhang, T.F. Xi, D.Y. Zhang, Surface modification of an Mg-1Ca alloy to slow down its biocorrosion by chitosan, Biomed Mater 4(4) (2009).
[33] H.M. Wong, K.W.K. Yeung, K.O. Lam, V. Tam, P.K. Chu, K.D.K. Luk, K.M.C. Cheung, A biodegradable polymer-based coating to control the performance of magnesium alloy orthopaedic implants, Biomaterials 31(8) (2010) 2084-2096.
[34] T. Zhang, Z. Tao, J. Chen, Magnesium–air batteries: from principle to application, Materials Horizons 1(2) (2014) 196-206.
[35] M. Long, H.J. Rack, Titanium alloys in total joint replacement - a materials science perspective, Biomaterials 19(18) (1998) 1621-1639.
[36] J.D. Bobyn, C.A. Engh, Human Histology of the Bone-Porous Metal Implant Interface, Orthopedics 7(9) (1984) 1410-1421.
[37] H.D. Jung, T.S. Jang, L. Wang, H.E. Kim, Y.H. Koh, J. Song, Novel strategy for mechanically tunable and bioactive metal implants, Biomaterials 37 (2015) 49-61.
[38] M. Niinomi, Recent metallic materials for biomedical applications, Metall Mater Trans A 33(3) (2002) 477-486.
[39] K.-H. Frosch, K.M. Stürmer, Metallic biomaterials in skeletal repair, European Journal of Trauma 32(2) (2006) 149-159.
[40] G. Rondelli, P. Torricelli, M. Fini, R. Giardino, In vitro corrosion study by EIS orthopaedic of a nickel-free stainless steel for applications, Biomaterials 26(7) (2005) 739-744.
[41] H.D. Jung, S.W. Yook, C.M. Han, T.S. Jang, H.E. Kim, Y.H. Koh, Y.

Estrin, Highly aligned porous Ti scaffold coated with bone morphogenetic protein-loaded silica/chitosan hybrid for enhanced bone regeneration, Journal of Biomedical Materials Research Part B: Applied Biomaterials 102(5) (2014) 913-921.
[42] V.H. Pham, S.H. Lee, Y. Li, H.E. Kim, K.H. Shin, Y.H. Koh, Utility of tantalum (Ta) coating to improve surface hardness in vitro bioactivity and biocompatibility of Co-Cr, Thin Solid Films 536 (2013) 269-274.
[43] R. Huiskes, H. Weinans, B. Vanrietbergen, The Relationship between Stress Shielding and Bone-Resorption around Total Hip Stems and the Effects of Flexible Materials, Clin Orthop Relat R (274) (1992) 124-134.
[44] M. Kanayama, B.W. Cunningham, C.J. Haggerty, K. Abumi, K. Kaneda, P.C. McAfee, In vitro biomechanical investigation of the stability and stress-shielding effect of lumbar interbody fusion devices, J Neurosurg 93(2) (2000) 259-265.
[45] H.D. Jung, H.E. Kim, Y.H. Koh, Production and evaluation of porous titanium scaffolds with 3-dimensional periodic macrochannels coated with microporous TiO2 layer, Mater Chem Phys 135(2-3) (2012) 897-902.
[46] S.B. Kim, J.H. Jo, S.M. Lee, H.E. Kim, K.H. Shin, Y.H. Koh, Use of a poly(ether imide) coating to improve corrosion resistance and biocompatibility of magnesium (Mg) implant for orthopedic applications, J Biomed Mater Res A 101(6) (2013) 1708-1715.
[47] J.H. Jo, J.Y. Hong, K.S. Shin, H.E. Kim, Y.H. Koh, Enhancing biocompatibility and corrosion resistance of Mg implants via surface treatments, J Biomater Appl 27(4) (2012) 469-476.
[48] S.M. Kim, J.H. Jo, S.M. Lee, M.H. Kang, H.E. Kim, Y. Estrin, J.H. Lee, J.W. Lee, Y.H. Koh, Hydroxyapatite-coated magnesium implants with improved in vitro and in vivo biocorrosion, biocompatibility, and bone response, J Biomed Mater Res A 102(2) (2014) 429-441.
[49] H.D. Jung, H.S. Park, M.H. Kang, S.M. Lee, H.E. Kim, Y. Estrin, Y.H. Koh, Polyetheretherketone/magnesium composite selectively coated with hydroxyapatite for enhanced in vitro bio-corrosion resistance and biocompatibility, Mater Lett 116 (2014) 20-22.
[50] J.H. Jo, Y. Li, S.M. Kim, H.E. Kim, Y.H. Koh, Hydroxyapatite/poly(epsilon-caprolactone) double coating on magnesium for enhanced corrosion resistance and coating flexibility, J Biomater Appl 28(4) (2013) 617-625.
[51] S.W. Kim, H.D. Jung, M.H. Kang, H.E. Kim, Y.H. Koh, Y. Estrin, Fabrication of Porous titanium scaffold with controlled porous structure and net-shape using magnesium as spacer, Mat Sci Eng C-Mater 33(5) (2013) 2808-2815.

[52] H.D. Jung, S.W. Yook, T.S. Jang, Y. Li, H.E. Kim, Y.H. Koh, Dynamic freeze casting for the production of porous titanium (Ti) scaffolds, Mat Sci Eng C-Mater 33(1) (2013) 59-63.
[53] K.G. Battiston, J.W.C. Cheung, D. Jain, J.P. Santerre, Biomaterials in co-culture systems: Towards optimizing tissue integration and cell signaling within scaffolds, Biomaterials 35(15) (2014) 4465-4476.
[54] G.C. Li, X.Y. Zhao, W.X. Zhao, L.Z. Zhang, C.P. Wang, M.R. Jiang, X.S. Gu, Y.M. Yang, Porous chitosan scaffolds with surface micropatterning and inner porosity and their effects on Schwann cells, Biomaterials 35(30) (2014) 8503-8513.
[55] J.H. Jo, B.G. Kang, K.S. Shin, H.E. Kim, B.D. Hahn, D.S. Park, Y.H. Koh, Hydroxyapatite coating on magnesium with MgF2 interlayer for enhanced corrosion resistance and biocompatibility, J Mater Sci-Mater M 22(11) (2011) 2437-2447.
[56] S. Hiromoto, A. Yamamoto, High corrosion resistance of magnesium coated with hydroxyapatite directly synthesized in an aqueous solution, Electrochim Acta 54(27) (2009) 7085-7093.
[57] M. Tomozawa, S. Hiromoto, Growth mechanism of hydroxyapatite-coatings formed on pure magnesium and corrosion behavior of the coated magnesium, Appl Surf Sci 257(19) (2011) 8253-8257.
[58] H. Wang, Y. Estrin, H. Fu, G. Song, Z. Zuberova, The effect of pre-processing and grain structure on the bio-corrosion and fatigue resistance of magnesium alloy AZ31, Adv Eng Mater 9(11) (2007) 967.
[59] X.N. Gu, N. Li, W.R. Zhou, Y.F. Zheng, X. Zhao, Q.Z. Cai, L.Q. Ruan, Corrosion resistance and surface biocompatibility of a microarc oxidation coating on a Mg-Ca alloy, Acta Biomater 7(4) (2011) 1880-1889.
[60] L.M. Chang, L.F. Tian, W. Liu, X.Y. Duan, Formation of dicalcium phosphate dihydrate on magnesium alloy by micro-arc oxidation coupled with hydrothermal treatment, Corros Sci 72 (2013) 118-124.
[61] M.H. Kang, H.D. Jung, S.W. Kim, S.M. Lee, H.E. Kim, Y. Estrin, Y.H. Koh, Production and bio-corrosion resistance of porous magnesium with hydroxyapatite coating for biomedical applications, Mater Lett 108 (2013) 122-124.
[62] C.E. Wen, Y. Yamada, K. Shimojima, Y. Chino, H. Hosokawa, M. Mabuchi, Compressibility of porous magnesium foam: dependency on porosity and pore size, Mater Lett 58(3-4) (2004) 357-360.
[63] C.E. Wen, M. Mabuchi, Y. Yamada, K. Shimojima, Y. Chino, T. Asahina, Processing of biocompatible porous Ti and Mg, Scripta Mater 45(10) (2001) 1147-1153.
[64] H.Y. Zhuang, Y. Han, A.L. Feng, Preparation, mechanical properties and

in vitro biodegradation of porous magnesium scaffolds, Mat Sci Eng C-Bio S 28(8) (2008) 1462-1466.
[65] J.X. Yang, F.Z. Cui, I.S. Lee, Surface Modifications of Magnesium Alloys for Biomedical Applications, Ann Biomed Eng 39(7) (2011) 1857-1871.
[66] J.P. Collier, V.A. Surprenant, M.B. Mayor, M. Wrona, R.E. Jensen, H.P. Surprenant, Loss of hydroxyapatite coating on retrieved, total hip components, J Arthroplasty 8(4) (1993) 389-93.
[67] K. Soballe, Hydroxyapatite ceramic coating for bone implant fixation. Mechanical and histological studies in dogs, Acta Orthop Scand Suppl 255 (1993) 1-58.
[68] T.F. Conceicao, N. Scharnagl, C. Blawert, W. Dietzel, K.U. Kainer, Corrosion protection of magnesium alloy AZ31 sheets by spin coating process with poly(ether imide) [PEI], Corros Sci 52(6) (2010) 2066-2079.
[69] T.F. da Conceicao, N. Scharnagl, W. Dietzel, K.U. Kainer, Corrosion protection of magnesium AZ31 alloy using poly(ether imide) [PEI] coatings prepared by the dip coating method Influence of solvent and substrate pre-treatment, Corros Sci 53(1) (2011) 338-346.
[70] N. Scharnagl, C. Blawert, W. Dietzel, Corrosion protection of magnesium alloy AZ31 by coating with poly(ether imides) (PEI), Surf Coat Tech 203(10-11) (2009) 1423-1428.
[71] T.S. Jang, E.J. Lee, J.H. Jo, J.M. Jeon, M.Y. Kim, H.E. Kim, Y.H. Koh, Fibrous membrane of nano-hybrid poly-L-lactic acid/silica xerogel for guided bone regeneration, J Biomed Mater Res B 100B(2) (2012) 321-330.
[72] S.H. Jun, E.J. Lee, S.W. Yook, H.E. Kim, H.W. Kim, Y.H. Koh, A bioactive coating of a silica xerogel/chitosan hybrid on titanium by a room temperature sol-gel process, Acta Biomater 6(1) (2010) 302-307.
[73] T.L. Nguyen, M.P. Staiger, G.J. Dias, T.B.F. Woodfield, A Novel Manufacturing Route for Fabrication of Topologically-Ordered Porous Magnesium Scaffolds, Adv Eng Mater 13(9) (2011) 872-881.
[74] T. Kokubo, H. Takadama, How useful is SBF in predicting in vivo bone bioactivity?, Biomaterials 27(15) (2006) 2907-2915.
[75] M. Rudert, Histological evaluation of osteochondral defects: consideration of animal models with emphasis on the rabbit, experimental setup, follow-up and applied methods, Cells Tissues Organs 171(4) (2002) 229-240.
[76] J. Čapek, D. Vojtěch, Effect of sintering conditions on the microstructural and mechanical characteristics of porous magnesium materials prepared by powder metallurgy, Materials Science and Engineering: C 35 (2014) 21-28.
[77] I. Morgenthal, O. Andersen, C. Kostmann, G. Stephani, T. Studnitzky, F.

Witte, B. Kieback, Highly porous magnesium alloy structures and their properties regarding degradable implant application, Adv Eng Mater 16(3) (2014) 309-318.
[78] Y. Bi, Y. Zheng, Y. Li, Microstructure and mechanical properties of sintered porous magnesium using polymethyl methacrylate as the space holder, Mater Lett 161 (2015) 583-586.
[79] J. Čapek, D. Vojtěch, Properties of porous magnesium prepared by powder metallurgy, Materials Science and Engineering: C 33(1) (2013) 564-569.
[80] G. Ryan, A. Pandit, D.P. Apatsidis, Fabrication methods of porous metals for use in orthopaedic applications, Biomaterials 27(13) (2006) 2651-2670.
[81] H. Camron, R. Pilliar, I. Macnab, The rate of bone ingrowth into porous metal, J Biomed Mater Res A 10(2) (1976) 295-302.
[82] J.A. Buckwalter, M.J. Glimcher, R.R. Cooper, R. Recker, Bone Biology .1. Structure, Blood-Supply, Cells, Matrix, and Mineralization, J Bone Joint Surg Am 77a(8) (1995) 1256-1275.
[83] J.Y. Rho, L. Kuhn-Spearing, P. Zioupos, Mechanical properties and the hierarchical structure of bone, Med Eng Phys 20(2) (1998) 92-102.
[84] S. Weiner, H.D. Wagner, The material bone: Structure mechanical function relations, Annu Rev Mater Sci 28 (1998) 271-298.
[85] V. Karageorgiou, D. Kaplan, Porosity of 3D biomaterial scaffolds and osteogenesis, Biomaterials 26(27) (2005) 5474-5491.
[86] D.R. Carter, W.C. Hayes, The compressive behavior of bone as a two-phase porous structure, The Journal of Bone & Joint Surgery 59(7) (1977) 954-962.
[87] S.A. Goldstein, The Mechanical-Properties of Trabecular Bone - Dependence on Anatomic Location and Function, J Biomech 20(11-12) (1987) 1055-1061.
[88] M.H. Kang, T.S. Jang, H.D. Jung, S.M. Kim, H.E. Kim, Y.H. Koh, J. Song, Poly(ether imide)-silica hybrid coatings for tunable corrosion behavior and improved biocompatibility of magnesium implants, Biomed Mater 11(3) (2016).
[89] S.H. Jun, E.J. Lee, H.E. Kim, J.H. Jang, Y.H. Koh, Silica-chitosan hybrid coating on Ti for controlled release of growth factors, J Mater Sci-Mater M 22(12) (2011) 2757-2764.
[90] A.I. Romero, M.L. Parentis, A.C. Habert, E.E. Gonzo, Synthesis of polyetherimide/silica hybrid membranes by the sol-gel process: influence of the reaction conditions on the membrane properties, J Mater Sci 46(13) (2011) 4701-4709.
[91] A. Abdal-hay, N.A.M. Barakat, J.K. Lim, Hydroxyapatite-doped

poly(lactic acid) porous film coating for enhanced bioactivity and corrosion behavior of AZ31 Mg alloy for orthopedic applications, Ceram Int 39(1) (2013) 183-195.
[92] T.G. Tihan, M.D. Ionita, R.G. Popescu, D. Iordachescu, Effect of hydrophilic–hydrophobic balance on biocompatibility of poly (methyl methacrylate)(PMMA)–hydroxyapatite (HA) composites, Mater Chem Phys 118(2) (2009) 265-269.
[93] A. Zomorodian, M.P. Garcia, T. Moura e Silva, J.C. Fernandes, M.H. Fernandes, M.F. Montemor, Corrosion resistance of a composite polymeric coating applied on biodegradable AZ31 magnesium alloy, Acta Biomater 9(10) (2013) 8660-70.
[94] E. Garcia-Gareta, M.J. Coathup, G.W. Blunn, Osteoinduction of bone grafting materials for bone repair and regeneration, Bone 81 (2015) 112-121.
[95] E.J. Lee, D.S. Shin, H.E. Kim, H.W. Kim, Y.H. Koh, J.H. Jang, Membrane of hybrid chitosan-silica xerogel for guided bone regeneration, Biomaterials 30(5) (2009) 743-50.
[96] H.D. Jung, S.W. Yook, C.M. Han, T.S. Jang, H.E. Kim, Y.H. Koh, Y. Estrin, Highly aligned porous Ti scaffold coated with bone morphogenetic protein-loaded silica/chitosan hybrid for enhanced bone regeneration, J Biomed Mater Res B 102(5) (2014) 913-921.
[97] N. Adden, Biodegradable metallic stent, Google Patents, 2009.
[98] T. Tsuji, H. Tamai, K. Igaki, E. Kyo, K. Kosuga, T. Hata, M. Okada, T. Nakamura, H. Komori, S. Motohara, Biodegradable Polymeric Stents, Current interventional cardiology reports 3(1) (2001) 10-17.
[99] H. Hermawan, D. Dubé, D. Mantovani, Developments in metallic biodegradable stents, Acta Biomater 6(5) (2010) 1693-1697.
[100] C. Di Mario, H. Griffiths, O. Goktekin, N. Peeters, J. Verbist, M. Bosiers, K. Deloose, B. Heublein, R. Rohde, V. Kasese, Drug-eluting bioabsorbable magnesium stent, Journal of interventional cardiology 17(6) (2004) 391-395.
[101] X.-N. Gu, Y.-F. Zheng, A review on magnesium alloys as biodegradable materials, Frontiers of Materials Science in China 4(2) (2010) 111-115.
[102] R. Erbel, C. Di Mario, J. Bartunek, J. Bonnier, B. de Bruyne, F.R. Eberli, P. Erne, M. Haude, B. Heublein, M. Horrigan, Temporary scaffolding of coronary arteries with bioabsorbable magnesium stents: a prospective, non-randomised multicentre trial, The Lancet 369(9576) (2007) 1869-1875.
[103] P. Zartner, M. Buettner, H. Singer, M. Sigler, First biodegradable metal stent in a child with congenital heart disease: evaluation of macro and histopathology, Catheterization and Cardiovascular Interventions 69(3) (2007) 443-446.

[104] M. Shechter, M. Sharir, M.J.P. Labrador, J. Forrester, B. Silver, C.N.B. Merz, Oral magnesium therapy improves endothelial function in patients with coronary artery disease, Circulation 102(19) (2000) 2353-2358.
[105] J.A. Maier, C. Malpuech-Brugère, W. Zimowska, Y. Rayssiguier, A. Mazur, Low magnesium promotes endothelial cell dysfunction: implications for atherosclerosis, inflammation and thrombosis, Biochimica et Biophysica Acta (BBA)-Molecular Basis of Disease 1689(1) (2004) 13-21.
[106] B. Dickens, W. Weglicki, Y.-S. Li, I. Mak, Magnesium deficiency in vitro enhances free radical-induced intracellular oxidation and cytotoxicity in endothelial cells, FEBS letters 311(3) (1992) 187-191.
[107] J. Wang, Y. He, M.F. Maitz, B. Collins, K. Xiong, L. Guo, Y. Yun, G. Wan, N. Huang, A surface-eroding poly(1,3-trimethylene carbonate) coating for fully biodegradable magnesium-based stent applications: Toward better biofunction, biodegradation and biocompatibility, Acta Biomater 9(10) (2013) 8678-8689.
[108] S.M. Kim, K.-S. Park, E. Lih, Y.J. Hong, J.H. Kang, I.H. Kim, M.H. Jeong, Y.K. Joung, D.K. Han, Fabrication and characteristics of dual functionalized vascular stent by spatio-temporal coating, Acta Biomater 38 (2016) 143-152.
[109] I. Iakovou, T. Schmidt, E. Bonizzoni, L. Ge, G.M. Sangiorgi, G. Stankovic, F. Airoldi, A. Chieffo, M. Montorfano, M. Carlino, Incidence, predictors, and outcome of thrombosis after successful implantation of drug-eluting stents, Jama 293(17) (2005) 2126-2130.
[110] J.A. Ormiston, P.W. Serruys, E. Regar, D. Dudek, L. Thuesen, M.W. Webster, Y. Onuma, H.M. Garcia-Garcia, R. McGreevy, S. Veldhof, A bioabsorbable everolimus-eluting coronary stent system for patients with single de-novo coronary artery lesions (ABSORB): a prospective open-label trial, The Lancet 371(9616) (2008) 899-907.
[111] C. Stettler, S. Wandel, S. Allemann, A. Kastrati, M.C. Morice, A. Schömig, M.E. Pfisterer, G.W. Stone, M.B. Leon, J.S. de Lezo, Outcomes associated with drug-eluting and bare-metal stents: a collaborative network meta-analysis, The Lancet 370(9591) (2007) 937-948.
[112] T. Xi, R. Gao, B. Xu, L. Chen, T. Luo, J. Liu, Y. Wei, S. Zhong, In vitro and in vivo changes to PLGA/sirolimus coating on drug eluting stents, Biomaterials 31(19) (2010) 5151-5158.
[113] C.J. Pan, J. Tang, Y. Weng, J. Wang, N. Huang, Preparation, characterization and anticoagulation of curcumin-eluting controlled biodegradable coating stents, Journal of Controlled Release 116(1) (2006) 42-49.
[114] X. Wang, S.S. Venkatraman, F.Y. Boey, J.S. Loo, L.P. Tan, Controlled

release of sirolimus from a multilayered PLGA stent matrix, Biomaterials 27(32) (2006) 5588-5595.
[115] P. Lu, H. Fan, Y. Liu, L. Cao, X. Wu, X. Xu, Controllable biodegradability, drug release behavior and hemocompatibility of PTX-eluting magnesium stents, Colloids and Surfaces B: Biointerfaces 83(1) (2011) 23-28.
[116] J. Li, P. Cao, X. Zhang, S. Zhang, Y. He, In vitro degradation and cell attachment of a PLGA coated biodegradable Mg–6Zn based alloy, J Mater Sci 45(22) (2010) 6038-6045.
[117] Y. Chen, Y. Song, S. Zhang, J. Li, C. Zhao, X. Zhang, Interaction between a high purity magnesium surface and PCL and PLA coatings during dynamic degradation, Biomed Mater 6(2) (2011) 025005.
[118] C. Schulz, M. von Rüsten-Lange, A. Krueger, A. Lendlein, F. Jung, Viability and function of primary human endothelial cells on smooth poly (ether imide) films, Clinical hemorheology and microcirculation 52(2-4) (2012) 267-282.
[119] Y. Chen, S.X. Zhang, J.A. Li, Y. Song, C.L. Zhao, X.N. Zhang, Dynamic degradation behavior of MgZn alloy in circulating m-SBF, Mater Lett 64(18) (2010) 1996-1999.
[120] C. Tan, D. Blackwood, Corrosion protection by multilayered conducting polymer coatings, Corros Sci 45(3) (2003) 545-557.

초록 (Abstract)

기능성 표면 코팅을 통한 의료용 생분해성 마그네슘 임플란트의 부식저항성 및 생체친화성 증진

서울대학교

재료공학부

강 민 호

생분해성 임플란트는 생체 내에서 서서히 분해되어 신체 조직의 회복 후 임플란트를 제거하기 위한 2 차 수술이 필요 없는 이상적인 의료용 임플란트로 주목 받고 있다. 생분해성 소재 중 마그네슘과 그 합금은 우수한 기계적 물성과 생체 적합성으로 생분해성 임플란트 소재로써 많은 연구가 진행되고 있으며 특히 치아, 정형외과용 그리고 혈관 스텐트 분야에서 활용하고자 연구되고 있다. 하지만 이러한 우수한 특성에도 불구하고 생체 환경 내에서의 급격한 부식이 일어나 마그네슘 임플란트는 임상 분야에서의 사용이 제한되고 있다. 따라서 마그네슘 임플란트의 기능성 표면 코팅 통해 부식 속도를 늦추고 나아가 생체 친화성을 증진시켜 궁극적으로 임플란트의 기능을 향상시켜야 한다.

첫 번째 연구에서는 치아 및 정형외과용 임플란트로 응용하기 위해 생체 모방형 마그네슘에 폴리에터르이미드-실리카 하이브리드를 코팅하였다. 실제 뼈의 구조와 구성 성분을 모방하여 높은 기공 연결성과 기계적 물성과 함께 우수한 뼈 전도성을 얻을 수 있다. 뼈는 조밀한 구조와 다공성 구조가 공존하여 밀도 대비 기계적 강도가 매우 높다. 더욱이, 하이드록시아파타이트가 주요 구성 성분 중 하나로 이 하이드록시아파타이트는 우수한 골 전도성을 지니고 있다. 방전 플라즈마 소결법과 염화나트륨을 기공 형성제로 사용하여 뼈의 구조를 모방한 마그네슘 스캐폴드를 제조할 수 있으며 이렇게 뼈 구조를 모방함으로서 마그네슘 임플란트는 높은 기공 연결성을 지니면서 높은 기계적 강도와 탄성률을 지닐 수 있다. 나아가 조밀한 구조의 비율을 조절함으로서 마그네슘 임플란트의 기계적 강도와 탄성률을 조절할 수 있다. 그리고 하이드록시아파타이트의 석출 코팅 공정을 통해 하이드록시아파타이트를 마그네슘 임플란트 표면에 코팅할 수 있다. 이러한 하이드록시아파타이트 코팅층은 마극네슘 임플란트의 부식 저항성과 골세포와의 생체적합성을 동시에 증진 시킬 수 있다. 하지만 하이드록시아파타이트의 brittle 한 특성으로 인해 코팅층 표면에 크랙과 같은 결함이 발생할 수 있으며 이러한 결함은 마그네슘 다공체의 복잡 형상과 넓은 표면적에 의해 마그네슘 임플란트의 부식과 생체 적합성에 치명적일 수 있다. 따라서 폴리에터르이미드-실리카 유-무기 하이브리드 층을 골 모방형 마그네슘 스캐폴드에 이중 코팅하였다. 폴리에터르이미드의 높은 부식 저항성과 실리카의 우수한 생체 적합성 및 활성도로 인해

골모방형 마그네슘의 부식 속도를 현저히 감소시킬 수 있었으며 나아가 골 조직의 생성을 촉진 시킬 수 있었다. 따라서 폴리에테르이미드-실리카 하이브리드가 코팅된 골모방형 마그네슘 임플란트는 치아 및 정형외과용 생분해성 스캐폴드로써 우수한 특성들을 지니고 있음을 확인 할 수 있었다.

두 번째 연구에서는 생분해성 약물 방출 스텐트 분야에 응용하기 위해 폴리에테르이미드/폴리락틱-co-글라이콜레이트 이중층을 마그네슘 스텐트의 표면 위치에 따라 선택적으로 코팅하였다. 마그네슘 스텐트는 혈관이 재생될 때 까지 스캐폴드의 지탱력을 유지하여야 하므로 부식 속도를 낮춰야 하며 더욱이 재협착을 방지하기 위해 항증식성 약물이 마그네슘 스텐트로부터 안정적으로 방출되어야 한다. 이러한 특성들을 만족시키기 위해 마그네슘 스텐트에 스프레이 코팅 공정을 통해 폴리에테르이미드/폴리락틱-co-글라이콜레이트 이중층을 스텐트의 외 · 내벽에 따라 선택적으로 코팅하였다. 마그네슘 스텐트의 부식을 억제하고 혈관표피세포와의 생체친화성을 향상시키기 위해 폴레에테르이미드가 스텐트 전면에 코팅되었다. 이어서 항증식성 약물인 시롤리무스가 담지된 폴리락틱-co-글라이콜레이트가 스텐트 외벽에 선택적으로 코팅되어 혈관 벽 쪽으로의 약물 방출을 유도하였다. 이러한 선택적 약물 방출은 혈관 근육 세포의 증식을 억제할 수 있으며 나아가 약물 방출에 따른 마그네슘 스텐트 내벽에서의 혈관 표피 세포에 미치는 악영향을 억제할 수 있다. 따라서 마그네슘 스텐트의 선택적 폴리에테르이미드/폴리락틱-co-글라이콜레이트 이중 코팅은 생분해성 약물 방출 스텐트 분야로서

적극 응용될 수 있음을 확인 할 수 있었다.

결과적으로 이러한 연구들은 응용분야에 따른 기능성 표면 코팅을 함으로서 마그네슘 임플란트의 부식 저항성과 생체 적합성을 증진시켜 궁극적으로 마그네슘 임플란트의 기능을 향상시킬 수 있었다. 분해 거동 평가와 세포 실험을 통해 폴리에테르이미드-실리카 하이브리드 코팅과 폴리에테르이미드/폴리락틱-co-글라이콜레이트 이중층의 선택적 코팅은 마그네슘 임플란트의 부식 저항성과 생체 특성을 효과적으로 증진시켜 치아/정형외과 분야와 혈관 스텐트 분야 임플란트로써 우수한 기능을 제공할 수 있음을 확인 할 수 있었다.

주요어: 마그네슘; 표면 코팅; 부식 저항성; 생체 적합성; 생체 활성; 하이드록시아파타이트; 폴리에테르이미드; 실리카 나노파티클; 다공성 스캐폴드; 폴리락틱-co-글라이콜레이트; 스텐트;

학번: 2011-23308